

The graphite deposit at Borrowdale (UK): a catastrophic mineralizing event associated with Ordovician magmatism

L. Ortega⁽¹⁾, D. Millward⁽²⁾, F. J. Luque^(1,*), J. F. Barrenechea⁽¹⁾, O. Beyssac⁽³⁾, J-M. Huizenga⁽⁴⁾, M. Rodas⁽¹⁾ and S. M. Clarke^(2, 5)

(1) Dpto. Cristalografía y Mineralogía, Facultad de Geología, Universidad Complutense de Madrid, 28040 Madrid, Spain.

(2) British Geological Survey, Murchison House, West Mains Road, Edinburgh EH9 3LA, UK.

(3) Laboratoire de Géologie, CNRS, Ecole Normale Supérieure, 24 rue Lhomond, 75005 Paris, France.

(4) School of Environmental Science and Development, North-West University, Potchefstroom, South Africa

(5) Current address: School of Physical and Geographical Sciences, Keele University, Keele ST5 5BG, UK

(*) Corresponding author: fluque@geo.ucm.es

Abstract

The volcanic-hosted graphite deposit at Borrowdale in Cumbria, UK was formed through precipitation from C-O-H fluids. The $\delta^{13}\text{C}$ data indicate that carbon was incorporated into the mineralizing fluids by assimilation of carbonaceous metapelites of the Skiddaw Group by andesite magmas of the Borrowdale Volcanic Group. The graphite mineralization occurred as the fluids migrated upwards through normal conjugate fractures forming the main subvertical pipe-like bodies. The mineralizing fluids evolved from $\text{CO}_2\text{-CH}_4\text{-H}_2\text{O}$ mixtures ($X_{\text{CO}_2}=0.6\text{-}0.8$) to $\text{CH}_4\text{-H}_2\text{O}$ mixtures. Coevally with graphite deposition, the andesite and dioritic wall rocks adjacent to the veins were intensely hydrothermally altered to a propylitic assemblage. The initial graphite precipitation was probably triggered by the earliest hydration reactions in the volcanic host rocks. During the main mineralization stage, graphite precipitated along the pipe-like bodies due to $\text{CO}_2 \rightarrow \text{C} + \text{O}_2$. This agrees with the isotopic data which indicate that the first graphite morphologies crystallizing from the fluid (cryptocrystalline aggregates) are isotopically lighter than those crystallizing later (flakes). Late chlorite-graphite veins were formed from CH_4 -enriched fluids

following the reaction $\text{CH}_4 + \text{O}_2 \rightarrow \text{C} + 2\text{H}_2\text{O}$, producing the successive precipitation of isotopically lighter graphite morphologies. Thus, as mineralization proceeded, water-generating reactions were involved in graphite precipitation, further favouring the propylitic alteration. The structural features of the pipe-like mineralized bodies as well as the isotopic homogeneity of graphite suggest that the mineralization occurred in a very short period of time.

1. INTRODUCTION

Most of the highest quality natural graphite used in industrial applications occurs as veins that crosscut their host rocks and therefore can be regarded as epigenetic. This category includes deposits of both current and past economic interest (e.g. Sri Lanka, India, New York, Montana, etc.). In such occurrences graphite is found along fracture systems and it is usually deposited from carbon-bearing fluids. In spite of the economic significance of this type of graphite deposit, little is known about the composition and characteristics of the fluids responsible for its formation. Thus, although fluid inclusions provide unique and direct information about the fluids involved in mineralization processes, there is only one reference on fluid inclusion studies in graphite deposits dealing with quartz–graphite veins hosted by metasedimentary rocks (Duke et al., 1990). More recently, Satish-Kumar (2005) has confirmed the usefulness of fluid inclusion studies to infer the mechanism of graphite precipitation and to model the carbon isotope evolution of the fluid–graphite system in granulites.

This paper characterizes the deposit at Seathwaite in Borrowdale, Cumbria (UK), where graphite was discovered. Mining there began at least as early as the late 16th century, and continued until the late 19th century, producing material for the casting of cannonballs, for coin moulds and as the basis for the renowned Keswick pencil industry. In addition to the historical interest of this deposit, it is also one of the only two large graphite occurrences known worldwide to be hosted by volcanic rocks, the other being at of Huelma in southern Spain (Barrenechea et al., 1997).

The origin of the Borrowdale graphite deposit has proved controversial, although even the earliest studies suggested the derivation from the assimilation of metapelitic rocks (Ward, 1876). Strens (1965) stated that graphite derived from the breakdown of carbon monoxide in the magmatic gases promoted by iron-bearing

minerals. Later, the deposit was regarded as epigenetic and graphite was considered to be derived from the assimilation of sedimentary organic matter (Weis et al., 1981). Parnell (1982) pointed to the relationship with granite intrusion in this area which promoted the mobilization of organic carbon compounds and the graphite mineralization. More recent works (Luque et al., 1998; Lindgren and Parnell, 2006) attributed the origin of the deposit to precipitation from carbon-bearing fluids. Luque et al. (2009) concluded that this is the first known volumetrically large fluid-deposited graphite occurrence formed at moderate temperature (~500 °C) in which graphite displays high crystallinity. In addition, the textural sequence of graphite morphologies and their isotopic analyses suggest precipitation from fluids with supersaturation in carbon decreasing progressively and the organic origin of the carbon in the mineralizing fluids (Barrenechea et al., 2009).

The aim of this work is to unravel the processes that led to the formation of this unique deposit. This paper integrates field evidence with new data from a fluid inclusion study and with the mineralogical and isotopic results from both the graphite deposit and its inferred carbon source (Skiddaw Group metapelites). Such an approach has provided a further insight into the progress of the mineralizing event and therefore a tool for understanding the mineralization processes in other fluid-deposited graphite occurrences.

2. GEOLOGIC BACKGROUND

The Borrowdale graphite deposit (Cumbria, UK) is hosted by andesite lavas and sills belonging to the Upper Ordovician (Katian) Borrowdale Volcanic Group (BVG), and by a probably contemporaneous hypabyssal dioritic intrusion (Fig. 1). The host BVG was emplaced during a brief magmatic episode that lasted no longer than 5 Ma (Millward and Evans, 2003). The subaerial, 6000 m-thick, caldera-related succession comprises basaltic to rhyolitic lavas, sills and pyroclastic rocks of medium- to high-K calc-alkaline, continental-margin, affinity (Beddoe-Stephens et al. 1995; Millward, 2004; Millward and Evans, 2003). The volcanic rocks are underlain by the upper Cambrian to Middle Ordovician Skiddaw Group, a succession of marine turbiditic mudstones and sandstones at least 5000 m thick (Cooper et al., 1995, 2004; Stone et al., 1999). Granitic plutons associated with the Caradoc volcanism intrude the Skiddaw and Borrowdale Volcanic Groups, and are inferred to be linked

to a granitic batholith concealed at a shallow depth (<4 km) beneath both groups (Lee, 1986). Clay mineral assemblages developed in the Skiddaw Group are consistent with early, very low grade metamorphism related to sedimentation and burial in an extensional basin where heat flow was quite high, possibly in the range 35-50 °C/km, and related to extensional, high heat-flow associated with volcanism and granitic batholith emplacement (Fortey, 1989; Fortey et al., 1993). Subsequent closure of the basin caused tectonic thickening with associated anchizonal to epizonal metamorphism (Soper and Woodcock, 2003; Merriman, 2006).

Several lines of evidence suggest that the Skiddaw Group rocks have contributed to the geochemical development of later aspects of Lake District geology. Firstly, the presence of garnet phenocrysts in peraluminous rocks in the BVG and associated intrusions (Fitton, 1972), and the isotope geochemistry of the rocks have been attributed to assimilation of pelitic material, most likely from the Skiddaw Group (McConnell et al., 2002). Secondly, sulfur isotope data from sulfides within the andesite rocks of the BVG also support this contention (Lowry et al., 1991). Finally, a zone of intense metasomatic alteration of the Skiddaw Group rocks in the northern Lake District is depleted in many of the elements, including carbon, that are concentrated in the varied mineral deposits of the Lake District, suggesting that these rocks could be the source of the carbon (Cooper et al. 1988). Metasomatic alteration is thought to be related to a concealed Acadian (c. 400 Ma) granitic intrusion (Cooper et al., 1988).

The age of graphite emplacement is poorly defined. The K-Ar ages of 382 and 376 Ma for the intrusion and vein deposit respectively (Mitchell and Ineson, 1975) are considered to have been reset like many others from the Lake District that have been determined by this method (Stone et al., 1999). A pre-Acadian age for the deposit is suggested by the presence of a pronounced cleavage in many hand specimens from the mine spoil heaps, but this fabric could not be traced in situ in the mine from the veins into the wall rock. The apparently direct association of the graphite with emplacement of the dioritic intrusion lead Millward (2004) to infer that the deposit was emplaced during Ordovician time; with the exception of the suite of Early Devonian lamprophyre dykes, all mafic intrusions in the Lake District are considered to have a Caradoc age.

3. MATERIALS AND ANALYTICAL METHODS

Samples from the graphite ore bodies, their volcanic host rocks and from the Skiddaw Group were studied in polished thin sections with a Zeiss Axiophot microscope under both transmitted and reflected light. Samples of graphite and the volcanic host rocks were collected along three of the old mine levels, that is, Gill's, Gilbert's and Farey's, and along the Grand Pipe (Fig. 2). In addition, some samples from the spoil heaps were also collected. Samples of pelitic Skiddaw Group rocks were collected from three of its formations (Loweswater, Kirk Stile, and Buttermere formations).

Fluid inclusions were studied in quartz fragments associated with graphite in the mineralized bodies. Microthermometric measurements were carried out at the Department of Crystallography and Mineralogy, Universidad Complutense, Madrid, on doubly polished sections, ~200 μm thick, using a Linkam THMS 600 heating-freezing stage, which is connected to a TMS92 programmable thermal control unit (temperature range between -190 and +600°C). The following temperatures were measured: (1) final melting and homogenization of the carbonic $\text{CO}_2\text{-CH}_4$ phase in mixed aqueous-carbonic inclusions: $T_{\text{H}_{\text{CAR}}} (\text{liq}_{\text{CAR}} + \text{vap} = \text{liq}_{\text{CAR}})$, respectively; (2) final melting temperature of ice in aqueous inclusions: $T_{\text{M}_{\text{ICE}}} (\text{ice} + \text{liq}_{\text{AQ}} + \text{vap} = \text{liq}_{\text{AQ}} + \text{vap})$; (3) clathrate melting: $T_{\text{M}_{\text{CL}}} (\text{liq}_{\text{CAR}} + \text{liq}_{\text{AQ}} + \text{cla} + \text{vap} = \text{liq}_{\text{CAR}} + \text{liq}_{\text{AQ}} + \text{vap})$; (4) total homogenization temperatures of mixed aqueous-carbonic inclusions: $T_{\text{H}_{\text{TOT}}} (\text{liq}_{\text{AQ}} + \text{liq}_{\text{CAR}} = \text{liq})$. Pure CO_2 and H_2O inclusions were used for calibration at the triple points (-56.6 and 0 °C). Measurements of $T_{\text{H}_{\text{CAR}}}$, $T_{\text{M}_{\text{ICE}}}$, $T_{\text{M}_{\text{CL}}}$ and $T_{\text{H}_{\text{CAR}}}$ have an accuracy of ~0.5°C.

Raman spectra of the carbonic species within the fluid inclusions were obtained using a Renishaw InVIA microspectrometer (ENS Paris) on the polished thin sections used for the petrographic study. We used a 514-nm Spectra Physics argon laser in circular polarization. The laser was focused on the sample by a DMLM Leica microscope with a 100 \times objective (Numerical aperture = 0.90), and the laser power at the sample surface was set around 1 mW. The Rayleigh diffusion was eliminated by edge filters, and the backscattered signal was finally dispersed using a 1800 lines-mm dispersive grating and analysed by a Peltier cooled RENCAM CCD detector. Under these conditions the spatial resolution is ~1 μm and the spectral resolution is close to 1 cm^{-1} . For the study of fluid inclusions the laser beam was focused within the inclusion and the spectra were recorded from 1200 to 1550 cm^{-1} and from 2700 to 3100 cm^{-1} using an acquisition time of 5 seconds and 10 accumulations. These conditions yielded a good signal/noise ratio to reach high definition of the CO_2 and CH_4 Raman bands, respectively. The Raman parameters (peak position, band intensity, and band area) were determined with the computer program PeakFit 3.0 using a Voigt function. Nitrogen was not found in any of the studied inclusions. Quantitative relative proportions of carbonic species were calculated from equations proposed by Dubessy et al. (1989).

Bulk composition, density and molar volume of the fluid inclusions (see next section for the detailed description of fluid inclusion types) were calculated from microthermometric and Raman data with the computer programs BULK, version 01/03 (for type V and L2 inclusions) and ICE, version 12/02 (for type L1 inclusions) (Bakker, 1997; Bakker, 2003; Bakker and Brown, 2003) using the Duan et al. (1992a, b) equation of state and considering NaCl as the only salt in solution. BULK was the preferred program for type V inclusions because clathrate was not visible in many of these inclusions,

notably those having low percentage of aqueous liquid phase at 20 °C. Salinity for type V inclusions with known clathrate melting temperature (T_{mCL}) was calculated with DENSITY, version 12/02 (Bakker, 1997; Bakker and Brown, 2003) and isocores for the same inclusions were determined using the program ISOC (Bakker, 2003; Bakker and Brown, 2003). For type L1 inclusions, in which the temperature of CO₂ homogenization (T_{hCAR}) was not available, an accurate measurement of T_{mCL} was required in order to use the ICE program. T_{mCL} was measured following cyclic heating–cooling runs. These runs consisted of cooling the inclusion down to -10 °C once the ice had melted to induce growth of the remaining clathrate phase, and increasing the upper limit of the heating temperature for every run in steps of +1 °C, until the clathrate was not observed further. The last recorded temperature limit was taken as the T_{mCL} . The salinity of L1 inclusions was estimated from the T_{mCL} data. L2 inclusions did not show either observable V–L transitions in the gas phase or clathrate melting, and an average bulk composition was estimated assuming a low density for the CH₄-rich gas phase.

Chemical compositions of minerals in the volcanic host rocks and within graphite nodules were analyzed by electron-microprobe (EMPA) using a JEOL Superprobe JXA 8900-M, under the following instrumental conditions: accelerating voltage of 15 kV, current of 20 nA, and beam diameter of 5 microns. Standards with similar compositions to the analyzed minerals were used (see Jarosewich et al., 1980, for details on the standard samples). Back-scattered electron (BSEM) images were recorded for the minerals analyzed.

XRD was performed on both graphite samples and Skiddaw Group metapelites. After grinding and homogenization of the samples to <53 µm, random-orientated powders were examined on a Siemens Kristalloflex 810 diffractometer, using Cu-Kα at 30 kV and 40 mA, a step size of 0.03 (°2θ), and time per step of 1 s (scan rate of 1.8° 2θ/min). In addition to the bulk mineralogy, the identification of clay minerals in the metapelites was carried out on orientated aggregates (OA) of the <2 µm fraction obtained by sedimentation onto glass slides from an aqueous suspension. For the identification of the clay minerals three types of OA were prepared: air dried, glycol-solvated, and heat treated at 550 °C. A slower scan rate (1.2 °2θ/min) was used between 2 and 13 °2θ in order to define peaks better. The full-width–half-maximum (FWHM) of the illite 10 Å peak (the so-called Kübler index, KI), was measured on the XRD patterns of the air-dried OA using the Diffrac Plus EVA 10.0 software. Our data (y) were transformed to Crystallinity Index Standard (CIS) data (x) (Warr and Rice, 1994) by the formula: $y = 1.2386x - 0.1259$. Therefore, KI values quoted in this study have been converted to the CIS scale, in which the anchizone limits are 0.25–0.42 °Δ2θ.

Carbonaceous material in samples SK-1 and SK-2 from the Skiddaw group was characterized by Raman microspectroscopy. Raman microspectroscopy was implemented to characterize the structural state of carbonaceous material in our samples and in order to obtain an estimate of the maximum temperature reached during metamorphism (RSCM, Raman Spectroscopy of Carbonaceous Material thermometry, Beyssac et al., 2002). Analytical conditions are described in detail in Beyssac et al. (2002, 2004).

The elemental carbon content of the Skiddaw metapelite samples was calculated using the total ion beam area (in units of amp-sec) generated from the isotope ratio mass spectrometry (IRMS) analysis. Each sample's total ion beam area (TBA) is compared with the TBA of the reference

standard, in this case cane sugar (42.10 %C). In addition, independent measurements of the carbon contents were carried out in a TOC-V CHS Shimadzu Total Organic Carbon (TOC) analyzer at the Faculty of Environmental Sciences (University of Castilla-La Mancha, Spain), equipped with a Shimadzu solid sample module SSM-5000A. Glucose was used as standard for calibration, and the precision of the measurements is within 1% of the determined amount of carbon. The analytical method consists of combustion and oxidation at a furnace temperature of 900 °C. Carrier gas was oxygen (99.9%), flowing at 500 mL/min. Elemental carbon analyses were done on powdered and homogenized samples of <53 and <25 µm.

Bulk stable carbon isotope analysis of graphite was performed at Geochron Laboratories (Massachusetts, USA). Samples were obtained from small holes excavated using a dentist's drill on unweathered surfaces of graphite nodules; although these powders contain silicate impurities, their graphite contents allowed for reproducible analyses. The analytical procedure was described in detail in a previous paper (Barrenechea et al., 1997).

Samples of Skiddaw Group metapelites were also analyzed at Iso-Analytical laboratories (Cheshire, UK) by EA-IRMS (elemental analyzer - isotope ratio mass spectrometry). Samples and references were weighed into tin capsules, sealed, and loaded into an auto-sampler on a Europa Scientific elemental analyzer. Samples were then dropped in sequence into a furnace held at 1000 °C and combusted in the presence of oxygen. The tin capsules flash combust, raising the temperature in the region of the sample to ~1700 °C. The combusted gases were swept in a helium stream over combustion catalyst (Cr_2O_3), copper oxide wires (to oxidize hydrocarbons), and silver wool to remove sulphur and halides. The resultant gases, N_2 , NO_x , H_2O , O_2 , and CO_2 were swept through a reduction stage of pure copper wires held at 600 °C. This removed any oxygen and converted NO_x species to N_2 . A magnesium perchlorate chemical trap was used to remove water. Nitrogen and carbon dioxide are separated using a packed column gas chromatograph held at a constant temperature of 100 °C. The resultant carbon dioxide peak entered the ion source of the Europa Scientific 20-20 IRMS where it was ionized and accelerated. Gas species of different mass were separated in a magnetic field and then simultaneously measured using a Faraday cup collector array to measure the isotopomers of CO_2 at m/z 44, 45, and 46. The analysis proceeded in a batch process by which a reference was analyzed followed by a number of samples and then another reference. The reference material used for analysis was IAEA-CH-6 ($\delta^{13}\text{C}_{\text{V-PDB}} = -10.43 \text{ ‰}$).

Four samples of pyrite-bearing andesite in which graphite nodules also appear were selected for sulphur isotope analysis to check for the source of sulphur. Calcite commonly overgrows the cubic pyrite crystals, so carbonate was removed from the igneous rock samples prior to analysis by acid digestion with 10 % hydrochloric acid at room temperature for 12 hours. Acid was removed by triple washing of the remaining sample material with de-ionized water prior to oven drying at 60 °C. Sample analysis was undertaken in duplicate by EA-IRMS at Iso-Analytical laboratories. Tin capsules containing reference or sample material plus vanadium pentoxide catalyst were loaded into an auto-sampler, from where they were dropped, in sequence, into a furnace held at 1080 °C and combusted in the presence of oxygen. Tin capsules flash combust, raising the temperature in the region of the sample to ca. 1700 °C. The combusted gases are then swept in a helium stream over combustion

catalysts (tungstic oxide/zirconium oxide) and through a reduction stage of high purity copper wires to produce SO₂, N₂, CO₂, and water. Water was removed using a Nafion™ membrane. Sulphur dioxide was resolved from N₂ and CO₂ on a packed GC column at a temperature of 32 °C. The resultant SO₂ peak entered the ion source of the IRMS where it was ionized and accelerated. Gas species of different mass were separated in a magnetic field then simultaneously measured on a Faraday cup universal collector array. Analysis was based on monitoring of m/z 48, 49 and 50 of SO⁺ produced from SO₂ in the ion source. The reference material used during analysis of the samples was IA-R036 (barium sulphate, $\delta^{34}\text{S}_{\text{V-CDT}} = +20.74 \text{ ‰}$). IA-R036, IA-R025 (barium sulphate, $\delta^{34}\text{S}_{\text{V-CDT}} = +8.53 \text{ ‰}$) and IA-R026 (silver sulphide, $\delta^{34}\text{S}_{\text{V-CDT}} = +3.96 \text{ ‰}$) were used for calibration and correction of the ¹⁸O contribution to the SO⁺ ion beam.

Chlorite from two chlorite–graphite veins was analysed for stable oxygen and hydrogen isotopes at the GNS Stable Isotopes Laboratory (New Zealand). In order to obtain chlorite concentrates, samples were crushed in a jaw-mill and ground further in a disc-mill. Then they were sieved to a 0.2-0.3 mm size. The resulting material was thoroughly washed and dried in a stove at 60 °C for 24 hours. Chlorite was then concentrated with a Frantz laboratory isodynamic magnetic separator (model L-1). The purity of the chlorite concentrates was checked by XRD. Oxygen was extracted from chlorite for isotope analyses using a CO₂-laser and BrF₅ (Sharp, 1990). Oxygen isotope values are reported in the familiar $\delta^{18}\text{O}$ notation, relative to V-SMOW. Samples were normalized to the garnet standard UWG-2 using a value of +5.8 ‰ (Valley et al., 1995). Values for three garnets varied by less than 0.1 ‰. Samples and standards were heated overnight to 150 °C in a muffle furnace (to remove adsorbed moisture) prior to loading onto the vacuum extraction line. Blank runs were done to ensure that yields were less than 0.1 µmoles oxygen. Oxygen yields of samples were recorded to ensure good oxygen yields and sample CO₂ gas was analysed on a Geo20-20 mass spectrometer.

Hydrogen isotope values of chlorite were obtained on an Isoprime mass spectrometer coupled with a Hekatek high temperature (ca. 1600 °C) analyser, configured for hydrogen isotope analyses. The results were normalised to IAEA CH-7 Polyethylene (-100.3 ‰) and IAEA NBS 30 biotite (-66 ‰). Precision for the hydrogen isotope measurements is better than 0.5 ‰.

Differential thermal analysis (DTA) and thermogravimetric (TG) curves of graphite were simultaneously recorded using a Seiko TG/TDA 320U apparatus. For these analyses the samples (gently ground and sieved to <53 µm) were heated at 10 °C/min in the range 20 °C to 1000 °C, with a continuous air supply of 50 ml/min. Under these conditions complete graphite combustion is guaranteed (Crespo et al., 2006). Alumina was used as reference material.

4. RESULTS

4.1. *The graphite deposit*

The Borrowdale graphite deposit occupies about a 400 m length of a conjugate set of normal faults hading up to 45°. Strens (1965) recorded five faults

striking 158–182° and three at 105°. Narrow veins and stringers filling the faults comprise massive graphite and chlorite along with quartz, but the richest deposits are developed at the intersections of the faults where there are steeply inclined pipe-like bodies up to 1 x 3 m in cross-section and from a few metres to over 100 m in length (Ward, 1876; Fig. 2). Graphite in the pipe-like bodies occurs as subspherical to ellipsoidal aggregates (nodules hereafter) and as irregular patches or small veins within altered andesite and dioritic host rocks (Fig. 3A). Nodules and patches may reach up to 10-15 cm in diameter or major length; their typical size is 1-2 cm, though nodules up to 1 m have been recorded (Ward, 1876). In places, graphite nodules are surrounded by greenish chloritic haloes (Fig. 3B). Rounded fragments of sandstone have been found in close association with the graphite nodules (Fig. 3C). In summary, graphite in the Borrowdale deposit occurs in three different contexts: i) as nodular masses within the pipe-like bodies, ii) along fault planes in the volcanic rocks, usually associated with chlorite, and iii) as replacements (disseminations) within the igneous host rocks.

A great diversity of graphite morphologies within the Borrowdale deposit has been recognized (Barrenechea et al., 2009). Graphite in the nodules and patches from the pipes mainly occur as 1) flakes (the most abundant morphology in the deposit, >90 %), 2) cryptocrystalline aggregates (mostly as colloform masses usually surrounded by flaky graphite), and 3) spherulites (5–40 µm in diameter, within laminar graphite). Composite nodules formed by cryptocrystalline graphite surrounded by flaky graphite have been found. Nodules and patches formed exclusively by flaky graphite frequently include radiating aggregates of elongate epidote crystals (Fig. 4A). The composition of the epidote is very homogeneous, corresponding to $\text{Ca}_2(\text{Mn}_{0.01}\text{Mg}_{0.01}\text{Fe}^{3+}_{0.75}\text{Ti}_{0.01}\text{Al}_{2.25})(\text{Al}_{0.02}\text{Si}_{2.98})\text{O}_{12}(\text{OH})$ or to Ps_{25} if expressed as the pistacite content (Table 1). Chlorite, polycrystalline quartz, pyrite, chalcopyrite and minor sericite may also occur within the graphite nodules.

Graphite in chlorite–graphite veins also appears with flaky (predominantly) and spherulitic morphologies. The composition of chlorite in the veins is given in Table 1. Chemical analyses point to two different chlorite compositions that are intimately associated forming fan-shaped aggregates (Fig. 4B). The H and O isotopic data for chlorite from the veins fall within very narrow ranges, with average values of $\delta^{18}\text{D}_{\text{V-SMOW}} = -63.4 \text{ ‰}$ and $\delta^{18}\text{O}_{\text{V-SMOW}} = 2.5 \text{ ‰}$, respectively (Table 1). $\delta\text{D}_{\text{H}_2\text{O}}$ values were calculated from the chlorite analyses using the fractionation relationship of Graham et

al. (1987), and $\delta^{18}\text{O}_{\text{H}_2\text{O}}$ values were calculated by extrapolation of the fractionation data given by Cole and Ripley (1998). The temperature used for these calculations (500 °C) was derived from a previous study (Luque et al., 2009).

The yellow-brown matrix within the mineralized pipe-like bodies comprises intensely altered wall rock and brecciated quartz. Also, both the andesite and dioritic wall rocks adjacent to the veins have been intensely hydrothermally altered to a propylitic assemblage containing quartz, chlorite, sericite and albite, along with some disseminated small aggregates of graphite and late calcite veinlets. Chlorite replaces the original ferromagnesian minerals, and sericite at least partially replaces the original plagioclase crystals. Chlorite compositions in the host rocks are more Mg-rich than those in the graphite–chlorite veins (Table 1). Graphite disseminations in the volcanic host rocks may occur as flakes, colloform aggregates, spherulites, and discs. Pyrite is also a common mineral in the andesite host rock, usually as subhedral to euhedral crystals (up to 2 mm long) which in places have been overgrown by small calcite or quartz crystals orientated perpendicular to the pyrite crystal faces (Fig. 3D). Sulfur isotope data of the pyrite range from $\delta^{34}\text{S}_{\text{V-CDT}} = 4.37$ to 6.99 ‰, in good agreement with previously published results of pyrite in andesite rocks from the BVG in this area (Lowry et al., 1991).

Graphite in the Borrowdale deposit displays very high crystallinity. XRD and Raman data (Luque et al., 2009) correspond to fully ordered hexagonal graphite with large crystallite sizes both along the stacking direction ($L_c=1110$ Å) and along the basal plane ($L_a>1000$ Å). Only colloform graphite grown over iron-bearing minerals (pyrite and silicates within the host rocks) has smaller in-plane crystallite sizes (L_a from 150 to 300 Å). In addition, thermal data indicate a high degree of crystallinity. The DTA curves show the exothermic maximum in the range from 747 to 771 °C (Fig. 5), comparable to other highly crystalline fluid-deposited graphites (Luque et al., 1998). Bulk carbon isotope data obtained from different parts of the nodules have $\delta^{13}\text{C}_{\text{PDB}}$ values ranging from -24.3 to -28.3 ‰. With few exceptions, $\delta^{13}\text{C}$ values are quite homogeneous within a single nodule (Fig. 6), and show small variations from samples collected at different points of the pipe-like bodies (Table 2). These results are in agreement with previously published bulk isotopic data for the Borrowdale graphite ($\delta^{13}\text{C} = -27.2$; Weis et al., 1981). However, bulk $\delta^{13}\text{C}$ values are slightly heavier than those reported for individual analyses of the most common graphite

morphology (flakes) within the nodules (average $\delta^{13}\text{C}_{\text{PDB}} = -30.26 \text{ ‰}$; Barrenechea et al., 2009).

4.2. Fluid inclusion study

Fluid inclusions were studied in quartz fragments associated with the graphite nodules in the mineralized pipes (Fig. 7A). The angular shape of the fragments and their well distributed occurrence, indicate that this quartz was brecciated, torn from its original location and transported upwards within the near vertical structures. Textural relationships between quartz and graphite (graphite nodules and patches commonly include quartz fragments and, less frequently, quartz encloses graphite crystals and aggregates; Barrenechea et al., 2009) suggest that the transport of quartz fragments along the pipes and graphite deposition were coeval. Therefore, fluid inclusions in the quartz fragments have recorded the fluids that were circulating during this event. The quartz fragments show an internal polycrystalline texture with individual grains containing abundant secondary inclusions (Figs. 7B and 7C). Sporadic grains are occasionally bounded by quartz recrystallized during the brecciation process. Therefore, fluid inclusions trapped in such recrystallized areas of the quartz grains have a primary origin (Figs. 7C and D).

The fluid inclusions can be grouped as low-density vapour-rich inclusions (V), and more dense liquid-rich inclusions (L). A closer examination of the relative volume of the aqueous phase at room temperature, along with microthermometric and Raman data, has allowed the definition of four types of inclusions: V, VS, L1 and L2 (Figs. 8 and 9). Detailed Raman, microthermometric and calculated bulk compositional data are summarized in Table 4.

Type V corresponds to two-phase vapour-rich inclusions ($V_v/V_t = 50\text{-}95\%$), made up of $\text{H}_2\text{O}-\text{CO}_2-\text{CH}_4$. These inclusions are relatively abundant and occur along trails within the clear cores of the quartz grains (Figs. 9A and 9B) and, less frequently as primary inclusions in growth bands of recrystallized quartz (Fig. 7D). However, in areas with a large number of inclusions, type V inclusions seem to be isolated within fields dominated by late L2 inclusions, which may have obliterated previous fluid inclusion assemblages. Raman data of the carbonic fraction in the type V inclusions indicate mixtures of CO_2-CH_4 , with $X_{\text{CO}_2} = 0.6\text{-}0.8$. Their average bulk carbonic content ($X_{\text{CO}_2}+X_{\text{CH}_4}$, mol fraction) varies from 0.8 in those inclusions with

$V_v/V_t > 0.9$, in which the water phase is difficult to see at room temperature, to 0.33 in inclusions having V_v/V_t between 0.6 and 0.8. The X_{H_2O} varies between 0.18 and 0.64, whereas the $X_{CO_2}/(X_{CO_2}+X_{CH_4})$ ratio ($\#X_{CO_2}$ hereafter) is rather constant, having an average value of 0.69 (Fig. 8). Final melting and liquid homogenization of the CO_2 - CH_4 phase ($n=46$) occurs between $-61.8\text{ }^{\circ}C$ and $-57.1\text{ }^{\circ}C$, and in the range $-23.6\text{ }^{\circ}C$ and $+7.9\text{ }^{\circ}C$, respectively. Clathrate melting temperatures between $+14.2$ and $+14.4$ indicate salinities up to 3 wt% eq. NaCl. Total homogenization of the inclusions ranges from 295 to $340\text{ }^{\circ}C$ (into vapour) and from 328 to $350\text{ }^{\circ}C$ (critical behaviour) indicating that the fluid was a vapour-like supercritical phase at the trapping conditions. Decrepitation prior to total homogenization at temperatures between 270 and $300\text{ }^{\circ}C$ is relatively common. The average density of this fluid type is 0.6 g cm^{-3} .

Type VS inclusions consist of a large bubble containing pure CH_4 vapour plus highly crystalline graphite and a liquid H_2O phase (up to 15 % vol.). These inclusions are very scarce (only three have been observed) and they occur closely associated with secondary trails of V and L1 inclusions (Fig. 9C and 9D), suggesting that these fluid inclusion types may be temporally and/or genetically related.

Type L1 are two-phase liquid-rich H_2O - CO_2 - CH_4 -bearing inclusions ($V_v/V_t = 25\text{--}40\%$). These are secondary inclusions and occur spatially associated with type V (Figs. 9E and 9F), although L1 are notably less abundant than V inclusions. Raman analysis indicate X_{CO_2} between 0.03-0.28 in most L1 inclusions ($n=6$) and a further three inclusions had $X_{CO_2}=0.5\text{--}0.62$, (Table 4). Although these three inclusions show $\#X_{CO_2}$ values close to type V inclusions (Fig. 10), they were classified as L1 because the volume of the vapour phase is <0.5 and they do not show CO_2 homogenization. Microthermometry on 23 inclusions gave values of $T_{m_{ICE}}$ in the interval $-7.5\text{ }^{\circ}C$ to $-4.2\text{ }^{\circ}C$ and $T_{m_{CL}}$ between $+9$ and $+16\text{ }^{\circ}C$. Bulk water content (mol fraction) is estimated to be >0.9 , with salinity ranging from 4 to 8 wt% eq. NaCl. Salinity values were derived from $T_{m_{CL}}$. Total homogenization occurs between 276 and $372\text{ }^{\circ}C$, similar to the homogenization temperatures for type V inclusions. However, whereas type V homogenizes either by bubble expansion or shows critical behaviour, L1 inclusions always homogenize into the liquid phase. The average density of L1 inclusions is $0.8\text{ cm}^3\text{ mol}^{-1}$.

Type L2 are two-phase liquid-rich inclusions ($V_v/V_t < 10\%$). They are very abundant and occur along trails (Fig. 9G) that occasionally cut across quartz grain

boundaries, thus indicating that the inclusions are secondary in origin and post-date the type V and L1 fluid circulation. They also occur in groups of numerous inclusions close to the subgrain boundaries of the quartz (Figs. 7C and 9H). CH₄ is the only carbonic species in these inclusions, with an estimated average composition (mol fraction) of 0.98 H₂O and 0.02 CH₄. Melting of ice occurs in the range -6 to -2.8 °C indicating salinities between 4.7 and 9.2 wt% NaCl. The total homogenization of the L2 inclusions (n=48) occurs between 160 and 205 °C, with a maximum in the interval 180-195 °C (n=25; Table 4).

4.3. Skiddaw Group metapelites

Samples from the Loweswater (SK-1), Kirk Stile (SK-2), and Buttermere formations (SK-3) within the Skiddaw Group show a well developed cleavage fabric. The mineral assemblages of these rocks consist of illite and chlorite, with subordinate amounts of quartz and trace amounts of K-feldspars. Both compositional and grain size banding are present with alternating light coloured bands composed mainly of very small particles of illite and quartz, and dark coloured bands consisting mainly of larger chlorite crystals and iron oxide. Small particles of carbonaceous matter also occur in both light and dark bands. Illite crystallinity (IK, CIS values) ranges from 0.15 ($\Delta^{\circ}2\theta$), for samples SK-1 and SK-2, to 0.31 ($\Delta^{\circ}2\theta$) for sample SK-3. These data are compatible with metamorphism at anchizonal to epizonal conditions, as previously suggested by Fortey (1989), Fortey et al. (1993) and Merriman (2006) for the whole Skiddaw Group.

The Raman study of carbonaceous material (CM) within the Skiddaw metapelites allowed the recognition of two main phases: a disordered pool and a highly graphitic one. The former is most abundant and corresponds texturally to organic matter transformed in situ during metamorphism, whereas the latter pool corresponds to detrital graphite (see Galy et al., 2008 for more details). Detrital particles are generally smaller than in situ CM but it is hard to define a size for in situ CM as it is generally texturally a continuous network. The spectra obtained for the in situ CM correspond to a maximum metamorphic temperature of 350 °C in both samples, with a standard error of less than ± 5 °C and a calibration attached accuracy of ± 50 °C (Beyssac et al., 2002), a very conservative estimate (cf. Beyssac et al., 2004).

Total organic carbon analyses in the Skiddaw Group samples studied reveal contents in the range from 0.31 to 0.86 % for the <25 µm samples. It is worth noting that samples ground to <53 µm show significantly lower carbon contents (0.19 to 0.36 %). This variation in the carbon content depending on the particle size is accompanied by a shift towards heavier $\delta^{13}\text{C}$ values (Table 3). The values presented here compare to the range of 0.039 to 0.59 % determined on a small number of typical Skiddaw Group rocks reported by Cooper et al. (1988).

5. DISCUSSION

The Borrowdale deposit is a unique example of a large volume of highly crystalline, fluid-deposited graphite emplaced in a subvolcanic environment. Such an association requires the coincidence of a number of special features in its formation, as discussed below.

The isotope composition of the fluid calculated from the chlorite data (Fig. 11) indicates mixing of a magmatic fluid with a probable component of surface-derived fluid (meteoric water), which is quite common in such environments (Henley and Hedenquist, 1986; Hedenquist and Masahiro, 1991; Hedenquist et al., 1994; Giggenbach, 1996; Giggenbach et al., 2003). The mineralization has an important tectonic control, with graphite occurring within near-vertical pipe-like bodies developed at the intersection of conjugate normal fractures which are also mineralized. These types of structure, especially the breccia pipes, imply an overpressured, fluid-rich regime which favoured the transport of andesitic and dioritic rocks and/or melts upwards and eventually resulted in the precipitation of huge amounts of graphite from such fluids. This fluid phase was recorded mostly as secondary inclusions in quartz xenoliths transported within the pipes.

5.1. Evolution of the fluids and timing of graphite precipitation

The fluid inclusion types in quartz associated with graphite in the Borrowdale deposit reveal the evolution of the carbon-bearing fluids involved in the mineralizing process. The petrographic analysis of the fluid inclusions, along with their composition (Figs. 9 and 10), allows the timing of fluid circulation to be established as follows: V → L1 → L2. However, although the type V and L2 inclusions are clearly

different and occur well separated in different secondary trails, the situation is not so clearly defined between V and L1. These two types of inclusion are spatially related (Figs. 9C, 9E and 9F) and some L1 inclusions show $\#XCO_2$ similar to the V fluid inclusion type (Fig. 10), thus suggesting that trapping of L1 inclusions probably took place shortly after V inclusions. The VS inclusions record a singular situation, located in time between the fluids represented by the V and L1 fluid inclusions, as will be discussed later.

According to the proposed chronology, the type V, vapour-rich fluid represents the fluid circulating at the earliest stages of the process. L1 inclusions, with low bulk carbonic content (< 0.1 mol fraction), plot outside the graphite stability field at any PT conditions and they likely represent the fluid compositional change during graphite precipitation. Therefore, the V fluid should be the initial fluid from which graphite started to precipitate. The composition of this fluid at the estimated PT conditions for the beginning of the mineralization process (500 °C and 2-3 kb; Luque et al., 2009) plots in the fluid + graphite field of the C-O-H diagram (Fig. 12), supporting the idea that it was saturated in graphite at the time of trapping. However, the lack of graphite crystals within type V inclusions suggests that the massive precipitation of graphite in the deposit had not started yet, thus implying that although the fluid was supersaturated with respect to carbon, it remained metastable for a short time. This situation is well known in crystals growing from solution, where the saturation of the fluid is a necessary, but not wholly sufficient condition for crystal growth: previously, nucleation of the solid phase must occur (Putnis et al., 1995). Therefore, massive graphite deposition should take place by the mass transfer of carbon from the carbonic fraction of the supersaturated type V fluid, once nucleation had occurred. Evidence of graphite morphologies corresponding to high supersaturation conditions in the Borrowdale deposit has been presented in a previous paper (Barrenechea et al., 2009). These morphologies, namely spherulites and cryptocrystalline colloform aggregates, represent the earliest stages of graphite nucleation, followed by flaky graphite as supersaturation decreased. Such a huge mineralizing event was recorded only by a few inclusions (the VS type), which trapped minute flakes of the newly crystallized graphite along with a drop of the coexisting fluid at the microscale. The close petrographic relationships among V, VS and L1 inclusions strongly suggest that bulk graphite precipitation took place in a very short period of time at the

geological scale. The latest stage of fluid circulation is represented by L2 inclusions, which correspond to the residual fluid once graphite precipitation had ceased.

The compositional trend of the fluid inclusion assemblages shows an overall fluid evolution characterized by: 1) depletion in the carbonic species, which were transferred to the solid state as graphite, and 2) progressive decrease in the $\#XCO_2$ from the early, oversaturated V fluid to the late L2 fluid which contains only minor CH_4 and no CO_2 . In detail, the V fluid records an increase in XH_2O with no change in the $\#XCO_2$ ratio (Fig. 10) thus remaining in the graphite saturation region (Fig. 12). In addition, the $\#XCO_2$ values of the post-graphite residual L1 fluid show two populations, one close to the V fluid and a second one ranging from 0.28 to 0.03. This evolution must reflect the conditions in which graphite precipitation took place and will be discussed later.

A significant aspect to be taken into account is that the initial composition of the graphite-depositing fluid (type V) is close to the solvus surface of the system at 500 °C (Diamond, 2003). Therefore, unmixing of aqueous and carbonic fluids might have occurred, enhanced by the pressure drop associated with the development of the pipes. The total homogenization temperatures of V and L1 within similar ranges (295-350 °C – into the vapour phase or critical –, and 276-370 °C – into the liquid phase –, respectively), along with the close spatial relationship among them, suggest that they could be derived from a boiling process. However, this hypothesis must be disregarded. L1- and V-type fluids cannot be the respective liquid and vapour fractions of a boiling fluid because $\#XCO_2$ is equal or even lower in L1 inclusions than in the V-type and this is against the carbonic species fractionation trend produced during unmixing of aqueous carbonic fluids (Ramboz et al., 1982). Furthermore, calculations made with the Geofluids Model 1 computer program (http://geotherm.ucsd.edu/geofluids/run_geofluids1.cgi, based on Duan et al., 1995) in order to model the phase status of a carbon-saturated fluid with $\#XCO_2 = 0.67$ and 1.4 % NaCl (Table 4) show no phase separation at $P = 2$ kbar and $T = 500$ °C, whereas an isothermal pressure drop from 2 kbar to 1 kbar would result in 0.197% liquid and 99.803% vapour. In practical terms, these results mean that the mineralizing fluid remained homogeneous at the given PT conditions estimated for graphite deposition. If pressure decreased as the mineralizing event proceeded, unmixing could have occurred, but this hardly could be recorded by a significant

number of fluid inclusions because of the very low relative proportion of the liquid phase as indicated by the above calculations.

5.2. Origin of carbon in the mineralizing fluids

The origin of carbon in C-O-H fluids can be recognized from the stable carbon isotope signatures of the precipitated graphite. The light isotopic signatures of both bulk graphite and of each of the different graphite morphologies from the Borrowdale deposit suggest that the carbon was derived from a biogenic source (Weis et al., 1981; Barrenechea et al., 2009).

There is geological and geochemical evidence of assimilation of Skiddaw Group metapelites by the volcanic host rocks (Fitton, 1972; Lowry et al., 1991; McConnell et al., 2002). Although inferred to have been caused by a later (Acadian) hydrothermal event, the presence of zones within the metapelites that have been depleted in carbon and other elements also supports this point (e.g. the Crummock Water zone, Fig. 1; Cooper et al., 1988). Therefore, Skiddaw metapelites must be regarded as the most probable source for carbon in the hydrothermal fluids responsible for the Borrowdale graphite deposit.

The bulk carbon isotopic analyses of Skiddaw metapelites yielded light $\delta^{13}\text{C}$ values within the typical range for biogenic carbonaceous matter. However, differences of 2 to 4 ‰ have been observed between the different particle size fractions studied. The <25 μm -fractions of the three samples studied in this paper (Table 3) show heavier isotopic ratios than their respective coarser fractions (>53 μm). This can be attributed to isotopic differences corresponding to various organic precursors, as frequently recognized in low-grade metamorphic samples (Grew, 1974; Okuyama-Kusunose and Itaya, 1987; Kribek et al., 1994). Alternatively, the presence of carbonaceous particles with heterogeneous graphitizing degrees in low-grade metamorphic rocks can be ascribed to the co-existence with detrital graphite (e.g. Buseck and Huang, 1985; Wada et al., 1994; Beyssac et al., 2003; Crespo et al., 2004; Rantitsch et al., 2004; Judik et al., 2008; Galy et al., 2008). For the Skiddaw metapelites, the detrital contribution is favoured by the textural and Raman data.

Considering the stable carbon isotope ratios for the dominant carbonaceous material within the Skiddaw metapelites (the largest particles, <53 μm , graphitized in

situ), the average $\delta^{13}\text{C}$ value is close to -28.5‰ . The assimilation at high temperature of such carbonaceous matter by the andesite magma produced isotopically heavier CO_2 . The fractionation between C and CO_2 at temperatures of about 1100 °C (the typical solidus temperature of andesite magmas) is $\alpha=5.5\text{‰}$ (Scheele and Hoefs, 1992). Thus, the isotopic signature of the CO_2 formed through assimilation of carbon from the Skiddaw metapelites would be -23‰ .

5.3. Conditions of graphite precipitation

Chemical reactions and P-T- $f\text{O}_2$ conditions of graphite precipitation have been inferred from mineral assemblage, fluid composition, and isotopic data.

Graphite nodules and patches within the pipes frequently include chlorite and radiating aggregates of elongate epidote crystals. Epidote is restricted to nodules exclusively composed of flaky graphite and shows a quite constant composition of Ps_{25} , indicating an oxygen fugacity buffered at the FMQ (Liou, 1993). Chlorite is related to both graphite spherulites and flaky graphite within the graphite–chlorite veins (Barrenechea et al., 2009). The andesite and dioritic wall rocks have also been intensely hydrothermally altered to an assemblage containing quartz, chlorite, and albite, along with some disseminated small aggregates of graphite and late calcite veinlets. These features are indicative of an intense propylitic alteration, and provide evidence that graphite precipitated during this hydrothermal event. Suitable PT conditions for graphite mineralization in the Borrowdale deposit have been estimated to be 2-3 kbar and 500 °C by Luque et al. (2009). Thermodynamic calculations carried out in this previous work show that carbon-saturated fluids with $\#X\text{CO}_2$ of 0.69 (type V fluid) and a $f\text{O}_2$ in equilibrium with the FMQ buffer are stable at temperatures of $\sim 500\text{ °C}$ for a pressure of 2-3 kbar. This pressure interval was considered the most likely, as it is compatible with an emplacement of the graphite deposit in a subvolcanic setting (Millward, 2004).

Formation of the graphite mineralization and propylitic alteration of the host rocks should have occurred during a short period of time. This is supported by geological and isotopic evidence, such as the structure of the deposit and the homogeneous carbon isotopic signature both at the microscale (Barrenechea et al., 2009) and at the scale of each single nodule. The brecciated, mineralized pipe-like bodies, containing sporadic clasts of Skiddaw Group lithologies, suggest rapid

transport of overpressured fluids upwards, similar to diatreme-like bodies. In addition, the isotopic signature of fluid-precipitated graphite is strongly dependent on 1) temperature, 2) bulk chemical composition of the fluid, and 3) oxygen fugacity (Duke and Rumble, 1986; Rumble et al., 1986; Luque et al., 1998; Farquhar et al., 1999). Any important change in one (or more) of these parameters implies relatively large isotopic variations. Thus, the existence of marked isotopic zoning is a common feature in fluid-deposited graphite at slow cooling rates (Luque et al., 1998; Binu-Lal et al., 2002; Santosh et al., 2003). For instance, Duke and Rumble (1986) showed that at $T=600\text{ }^{\circ}\text{C}$ and $P=3\text{ kbar}$, for compositions close to the water maximum of the C-O-H system, a variation of 0.4 log units $f\text{O}_2$ causes an isotopic shift of 5.1 ‰ in the graphite deposited. Similarly, for CO_2 -rich aqueous fluids, a small variation from $X\text{H}_2\text{O}=0.84$ to $X\text{H}_2\text{O}=0.79$ leads to an isotopic shift of 4.6 ‰. Given the similarity of the C-O-H diagram at the above PT conditions and at those estimated for the Borrowdale deposit, similar quantitative variations could be expected. However, the isotopic signatures among the different graphite morphologies do not differ by more than 3 ‰ (Barrenechea et al., 2009). In addition, very small isotopic heterogeneities (usually less than 1.5 ‰) are observed in samples taken from a given nodule (Fig. 6, Table 3). All these observations allow us to infer that graphite deposition within the pipes occurred very rapidly from a C-O-H fluid and under more or less constant $f\text{O}_2$.

Among the reactions involving CO_2 and CH_4 from which graphite can precipitate from a C-O-H fluid we can consider the following (Frost, 1979; Ohmoto and Kerrick, 1977): 1) $\text{CO}_2 + \text{CH}_4 \rightarrow 2\text{C} + 2\text{H}_2\text{O}$, 2) $\text{CO}_2 \rightarrow \text{C} + \text{O}_2$, and 3) $\text{CH}_4 + \text{O}_2 \rightarrow \text{C} + 2\text{H}_2\text{O}$. Reaction (1) between CH_4 and CO_2 is kinetically very sluggish. Furthermore, reaction 1 would not change $\#\text{CO}_2$, which contradicts our observations. The close relationship between epidote and flaky graphite within the pipes strongly suggests that the main graphite precipitation event started following the reaction $\text{CO}_2 \rightarrow \text{C} + \text{O}_2$. Epidote is not stable for $X\text{CO}_2 > 0.2$ (Liou, 1993) and the type V fluid contains an average bulk $X\text{CO}_2$ of 0.24. Therefore, epidote crystallization was likely triggered by the consumption of CO_2 in the graphite precipitation reaction. VS inclusions containing graphite along with $\text{CH}_4 + \text{H}_2\text{O}$ may be recording this reaction. The mechanism inducing initial nucleation and subsequent growth of cryptocrystalline and spherulitic graphite previous to epidote crystallization could be the early hydrothermal alteration of the host rocks, notably to form chlorite. It is well known that hydration reactions promote the precipitation of graphite, because the remaining fluid

is relatively enriched in C thus driving its composition into the stability field of graphite+fluid (Duke and Rumble, 1986; Luque et al., 1998; Farquhar et al., 1999). Such hydration reactions would be responsible for the occurrence of chlorite and epidote associated with graphite in the deposit. During this process of hydration, the fluid oxygen fugacity will decrease slightly but remain near the FMQ buffer value, which is an additional indication that the first graphite precipitation reaction should involve the reduction of CO_2 . In summary, initial graphite precipitation was promoted by the earliest hydration reactions leading to chlorite formation within the propylitic assemblage. Graphite morphologies related to this stage would comprise disseminated spherulites and cryptocrystalline (colloform) aggregates (Barrenechea et al., 2009). The consumption of CO_2 in the fluid as the result of graphite deposition would permit the subsequent crystallization of epidote associated with graphite morphologies (flakes) corresponding to lower supersaturation conditions.

Therefore, the dominant reaction of graphite crystallization within the pipes was $\text{CO}_2 \rightarrow \text{C} + \text{O}_2$. However, this reaction needs to be coupled with an oxygen-consuming reaction during graphite deposition to buffer the $f\text{O}_2$, because the composition of the epidote, notably the content in Fe^{3+} expressed as the pistacite content, is extremely sensitive to $f\text{O}_2$ conditions (Liou, 1993). Since fluid inclusion data reveal a progressive enrichment in water as graphite precipitation proceeded, the reaction $\text{CH}_4 + \text{O}_2 \rightarrow \text{C} + 2\text{H}_2\text{O}$ is considered as the most likely to have occurred. Such a reaction would have consumed the O_2 produced by the main reaction, thus maintaining the overall $f\text{O}_2$ conditions close to the FMQ buffer. This process is shown in Figure 12. The reduction of CO_2 results in a decrease of $\#\text{CO}_2$ and an increase in XH_2O (traject 1 in Fig. 12). During a later stage, the oxidation of CH_4 becomes the dominant graphite precipitation reaction (traject 2). This change in reaction is indicated by the curvature of the iso-oxygen fugacity lines in Figure 12. During this process, the buffering capacity of the rock would have contributed to keeping $f\text{O}_2$ conditions fairly constant by other coupled reactions. For instance, Strens (1965) reported the presence of hematite cores and rims formed after pyrite within graphite nodules. The absence of important changes in the $f\text{O}_2$ conditions is also supported by the lack of significant isotopic variations in the precipitated graphite, as previously mentioned. Both the reduction of CO_2 and the oxidation of CH_4 result in a change of $\#\text{CO}_2$. This change is indicated in Figure 12, and reflected in the $\#\text{CO}_2$ of type L1

inclusions. Typical of the fluid compositional change is that the fluid fO_2 remains constant near FMQ (Fig. 12).

Local heterogeneities probably occurred in the relative contribution of the reactions proposed above to the graphite precipitation process. As stated earlier, the $\#XCO_2$ values of the post-graphite residual L1 fluid show two populations, one close to the V fluid and a second one progressively poorer in CO_2 (Fig. 10). Similar $\#XCO_2$ ratios in V and L1 inclusions would represent areas of the deposit with equal contribution of both reactions, whereas the decreasing trend in $\#XCO_2$ would indicate sections of the pipes where the CO_2 consuming reaction was dominant. These changes are recorded in the isotopic signature of the precipitated graphite. Considering the isotopic signature of the assimilated carbon by the andesite magma ($\delta^{13}C = -23\text{‰}$) and the fractionation factor for CO_2 -C of 10.5 ‰ (Bottinga, 1969) at the temperature estimated for graphite precipitation ($\sim 500\text{ °C}$; Luque et al., 2009), graphite deposited from the initial CO_2 -rich fluid should have an isotopic signature close to -33.5‰ . This is in good agreement with the isotopic data for the earliest morphology crystallizing in the pipe-like bodies (i.e. colloform graphite with $\delta^{13}C = -33.7\text{‰}$; Barrenechea et al., 2009). The small isotopic variation among the different graphite morphologies and with respect to the bulk analysis of graphite nodules could be attributed to the evolution of the mineralizing C-O-H fluid. Thus, the local changes in the relative contributions of the graphite precipitation reactions would result in the observed isotopic heterogeneities, because such reactions influenced not only the relative amounts of carbon species in the fluid but also the XH_2O (Fig. 13). Fluids progressively poorer in CO_2 (or richer in H_2O and CH_4 as CO_2 was being consumed in the graphite-generating reaction, see Fig. 12) would lead to successive graphite crystals enriched in the heavy isotope (i.e. the flaky graphite within nodules, $\delta^{13}C = -30.2\text{‰}$; Barrenechea et al., 2009). In this scenario, the hydration reactions of the host rocks during their coeval propylitic alteration could also contribute to the limited isotopic heterogeneity of graphite. Within the late chlorite-graphite veins, the morphologies corresponding to higher supersaturation (i.e. spherulites) are isotopically heavier than those formed under lower supersaturation (i.e. flakes). This trend suggests that graphite in the chlorite-graphite veins mainly crystallized following reaction (3). In summary, the overall fluid system would have progressed towards the total consumption of CO_2 and most of the CH_4 , as recorded by L1 inclusions with $\#XCO_2 \sim 0.03$ and by the latest L2 inclusion assemblage.

5.4. Controls on the emplacement of the graphite deposit

The key role of the hypabyssal dioritic intrusion in the emplacement of the Borrowdale graphite deposit is amply demonstrated by their close relationship, as shown first by Strens (1965). As previously mentioned, the BVG represents subaerial, subduction-related andesitic volcanism and associated high-level intrusions in which the assimilation of carbonaceous metapelitic rocks has been implicated (e.g. McConnell et al., 2002). In the volcanic environment, the carbonic species derived from the assimilation would be released during magma ascent, and transferred to the surface, probably through the fault network (Giammanco et al., 1998). There is growing evidence from melt inclusions that many magmas are vapour saturated at 10-15 km depth and that a significant proportion of this is CO₂ (Lowenstern, 2001; Wallace, 2005). According to Giggenbach (1996), volatile contents of andesitic magmas related to subduction zones (like the BVG) are likely to be high enough to allow a separate, volatile-rich phase to be present during all stages of magma generation and migration.

By contrast with the high-level volcanic setting, the crystallization of a batch of magma under subvolcanic-hypabyssal conditions at Seathwaite (i.e. the dioritic intrusion) provided a completely different scenario, with rapid magma ascent preventing the loss of the volatiles (mostly CO₂, CH₄ and H₂O) generated during assimilation. In the dioritic intrusion at Seathwaite, the crystallization of the primary anhydrous mineral assemblage (clinopyroxene, orthopyroxene and plagioclase; Strens, 1965) caused the residual magma to become enriched in volatiles. This led to an increase in the vapour pressure which eventually overcame the confining lithostatic pressure promoting the hydraulic fracturing (brecciation) of the host rock. In turn, the expansion of the volatiles triggered the upwards movement of andesitic and dioritic rocks and/or melt, quartz fragments, and a supercritical carbon-rich fluid (represented by the V inclusions) that resulted in the formation of the breccia pipe bodies. This C-O-H fluid remained metastable until the earliest hydration reactions triggered the nucleation of the first graphite crystals (spherulites and colloform aggregates). This initial stage was followed by massive precipitation of graphite coupled with the pervasive propylitic alteration of the host rocks. As previously discussed, the structural and isotopic evidence indicate that the whole mineralization

process in Borrowdale was catastrophic, that is, it occurred in a geologically very short period of time.

Given the association with mafic intrusions, why is graphite mineralization restricted to the Seathwaite location? A significant number of hypabyssal mafic bodies of similar composition have been mapped throughout the Skiddaw Group outcrop to the north of Borrowdale (Fortey et al., 1994), yet none of these is known to have associated graphite deposits, nor have the few intrusions of this type that occur within the BVG outcrop (British Geological Survey 1:50 000-scale bedrock geological sheets 29, Keswick, and 38, Ambleside, 1999 and 1996 respectively). The answer may be the unique location of the Borrowdale intrusion in the immediate hanging wall of the Burtness Comb Fault (Fig. 1). This E- to ENE-striking fault with hade to the south, is inferred to lie above a repeatedly re-activated, deep-seated basement structure, and hence was one of the fundamental faults that controlled accumulation and preservation of the BVG (Millward, 2002). The fault may in part also mark the northern margin of the Scafell Caldera, a major piecemeal, hydrovolcanic system within the BVG (Branney and Kokelaar, 1994). Furthermore, faults with the same orientation as the graphite–chlorite veins at Seathwaite are known to have been involved in the volcanotectonic formation within the central part of the Scafell Caldera. Such active fault systems would have provided the necessary channel ways for the rapid ascent of both magma and C–O–H fluids.

6. CONCLUSIONS

The graphite deposit at Borrowdale is a unique type of mineralization in many aspects. Volcanic environments do not usually provide suitable conditions for the formation of volumetrically large graphite deposits. For this deposit to be formed an unusual combination of geological factors therefore occurred, including 1) the assimilation of carbonaceous matter by andesite magmas, 2) the existence of hypabyssal dioritic intrusions that prevented the loss of volatiles generated during assimilation as commonly occurs in volcanic environments, and 3) the singular occurrence at Seathwaite of one of these intrusions in the vicinity of an active fault system, which provided the channelways for the flow of the C–O–H fluids.

The importance of tectonic control on the mineralization is emphasized further by the occurrence of graphite within near-vertical pipe-like bodies developed at the

intersection of conjugate normal fractures which are also mineralized. Graphite mineralization and propylitic alteration of the volcanic host rocks in the Borrowdale deposit were intimately related. Both processes appear to have occurred in a short period of time. The mineralized breccia pipe bodies suggest a quick upwards transport of overpressured fluids, similar to diatreme-like bodies. The homogeneous carbon isotopic signature both at the microscale and at the scale of each single graphite nodule also implies rapid deposition. Graphite precipitation started at ~500 °C and about 2-3 kbar from CO₂-rich fluids. The initial graphite precipitation was probably triggered by the earliest hydration reactions leading to chlorite formation within the propylitic assemblage. As mineralization proceeded, water-generating reactions were involved in graphite precipitation from fluids progressively richer in methane relative to carbon dioxide, thus resulting in the widespread propylitic alteration of the host rock. The ultimate source of carbon in the mineralizing fluids was the carbonaceous matter contained in the Skiddaw Group metapelites that were assimilated by the andesite magmas of the Borrowdale Volcanic Group.

Acknowledgements

We thank Dr. R. Rojas (Institute of Materials Science, Madrid), Dr. J. Alonso-Azcárate (Faculty of Environmental Sciences, University of Castilla-La Mancha), and B. Soutullo for technical assistance during DTA-TG, TOC, and XRD analyses, respectively. We also acknowledge C. Valdehita for helping with the concentration of chlorite from chlorite-graphite veins for the stable isotope studies. Thanks are also due to Jeff Wilkinson and Dave Bridge who took care of our safety during the underground work and guided us through the labyrinthine stages of the old graphite mine. The National Trust is also thanked for providing access to the mine. The graphite mine is both a Scheduled Ancient Monument and a Site of Special Scientific Interest: permission to collect samples there was granted by the Secretary of State for Culture and Media and by Natural England respectively. This paper is a contribution from project CGL2006-00835 of the Spanish Ministry of Science and Innovation. David Millward publishes with the permission of the Executive Director, British Geological Survey (N.E.R.C.). This study was partly funded by INSU DyETI and ANR JC (GeoCarbons project) to Olivier Beyssac.

REFERENCES

- Bakker R. J. (1997) CLATHRATES: computer programs to calculate fluid inclusion: V–X. Properties using clathrate melting temperatures. *Comput. Geosci.* **23**, 1-18.
- Bakker R. J. (2003) Package FLUIDS 1. Computer programs for analysis of fluid inclusion data and for modelling bulk fluid properties. *Chem. Geol.* **194**, 3-23.
- Bakker R. J. and Brown P. E. (2003) Computer modelling in fluid inclusion research. In *Fluid Inclusions: Analysis and Interpretation* (eds. I. Samson, A. Anderson and D. Marshall). Mineralogical Association of Canada, Short Course series **32**, 175-212.
- Barrenechea J. F., Luque F. J., Millward D., Ortega L., Beyssac O. and Rodas M. (2009) Graphite morphologies from the Borrowdale deposit (NW England, UK): Raman and SIMS data. *Contrib. Mineral. Petrol.* **158**, 37-51.
- Barrenechea J. F., Luque F. J., Rodas M. and Pasteris J. D. (1997) Vein-type graphite mineralization in the Jurassic volcanic rocks of the external zone of the Betic Cordillera (Southern Spain). *Can. Miner.* **35**, 1379-1390.
- Beddoe-Stephens B., Petterson M. G., Millward D. and Marriner G. F. (1995). Geochemical variation and magmatic cyclicity within an Ordovician continental-arc volcanic field: the lower Borrowdale Volcanic Group, English Lake District. *J. Volcanol. Geotherm. Res.* **65**, 81-110.
- Beyssac O., Goffé B., Chopin C. and Rouzaud J-N. (2002) Raman spectra of carbonaceous material from metasediments: a new geothermometer. *J. Metamorphic Geol.* **20**, 859-871.
- Beyssac O., Goffé B., Petitet J-P., Froigneux E., Moreau M. and Rouzaud, J-N. (2003) On the characterization of disordered and heterogeneous carbonaceous materials by Raman spectroscopy. *Spectrochim. Acta Part A* **59**, 2267-2276.
- Beyssac O., Bollinger L., Avouac J. P. and Goffé B. (2004) Thermal metamorphism in the lesser Himalaya of Nepal determined from Raman spectroscopy of carbonaceous material. *Earth Planet. Sci. Lett.* **225**, 233-241.
- Binu-Lal S. S., Kehelpannala K. V. W., Satish-Kumar M. and Wada, H. (2002) Multistage graphite precipitation through protracted fluid flow in sheared metagranitoid, Digana, Sri Lanka: evidence from stable isotopes. *Chem. Geol.* **197**, 253-270.

- Bottinga Y. (1969) Calculated fractionation factors for carbon and hydrogen isotope exchange in the system calcite-carbon dioxide-graphite-methane-hydrogen-water vapor. *Geochim. Cosmochim. Acta* **33**, 49-64.
- Branney, M. J. and Kokelaar, B. P. (1994) Volcanotectonic faulting, soft-state deformation and rheomorphism of tuffs during development of a piecemeal caldera, English Lake District. *Geol. Soc. Am. Bull.* **106**, 507-530.
- Buseck P. R. and Huang B. J. (1985) Conversion of carbonaceous material to graphite during metamorphism. *Geochim. Cosmochim. Acta* **49**, 2003-2016.
- Cole D. R. and Ripley E. M. (1998) Oxygen isotope fractionation between chlorite and water from 170 to 350 °C: A preliminary assessment based on partial exchange and fluid/rock experiments. *Geochim. Cosmochim. Acta* **63**, 449-457.
- Cooper A. H., Rushton A. W. A., Molyneux S. G., Hughes R. A., Moore R. M. and Webb B. C. (1995) The stratigraphy, correlation, provenance and paleogeography of the Skiddaw Group (Ordovician) in the English Lake District. *Geol. Mag.* **132**, 185-211.
- Cooper A. H., Fortey N. J., Hughes R. A., Molyneux S. G., Moore R. M., Rushton A. W. A., Stone P., Allen P. M., Cooper D. C., Evans J. A., Hirons S. R. and Webb B. C. (2004) The Skiddaw Group of the English Lake District. *Mem. British Geol Surv*, London: HMSO.
- Cooper D. C, Lee M. K., Fortey N. J., Cooper A. H., Rundle C. C., Webb B. C. and Allen P. M. (1988) The Crummock Water aureole: a zone of metasomatism and source of ore metals in the English Lake District. *J. Geol. Soc., London* **145**, 523-540.
- Crespo E., Luque F. J., Fernández-Rodríguez C., Rodas M., Díaz-Azpiroz M., Fernández-Caliani J. C. and Barrenechea J. F. (2004) Significance of graphite occurrences in the Aracena Metamorphic Belt, Iberian Massif. *Geol. Mag.* **141**, 687-697.
- Crespo E., Luque F. J., Barrenechea J. F. and Rodas M. (2006) Influence of grinding on graphite crystallinity from experimental and natural data: implications for graphite thermometry and sample preparation. *Min. Mag.* **70**, 697-707.
- Diamond L. W. (2003) Introduction to gas-bearing, aqueous fluid inclusions. In *Fluid Inclusions: Analysis and Interpretation* (eds. I. Samson, A. Anderson and D.

- Marshall). Mineralogical Association of Canada, Short Course Series **32**, pp. 101-158.
- Duan Z., Møller N. and Weare J. H. (1992a) An equation of state for the CH₄-CO₂-H₂O system: I. Pure systems from 0 to 1000 °C and 0 to 8000 bar. *Geochim. Cosmochim. Acta* **56**, 2605–2617.
- Duan Z., Møller N. and Weare J. H. (1992b) An equation of state for the CH₄-CO₂-H₂O system: II. Mixtures from 50 to 1000 °C and 0 to 1000 bar. *Geochim. Cosmochim. Acta* **56**, 2619-2631.
- Duan Z., Møller N. and Weare J. H. (1995) Equation of state for the NaCl-H₂O-CO₂ system: Prediction of phase equilibria and volumetric properties. *Geochim. Cosmochim. Acta* **59**, 2869-2882.
- Dubessy J., Poty B. and Ramboz C. (1989) Advances in C-O-H-N-S fluid geochemistry based on micro-Raman spectrometric analysis of fluid inclusions. *Eur. J. Mineral.* **1**, 517-534.
- Duke E. F., Galbreath K. C. and Trusty K. J. (1990) Fluid inclusion and carbon isotope studies of quartz-graphite veins, Black Hills, South Dakota and Ruby Range, Montana. *Geochim. Cosmochim. Acta* **54**, 683-698.
- Duke E. F. and Rumble D. (1986) Textural and isotopic variations in graphite from plutonic rocks, South-Central New Hampshire. *Contrib. Mineral. Petrol.* **93**, 409-419.
- Farquhar J., Hauri E. and Wang J. (1999) New insights into carbon fluid chemistry and graphite precipitation: SIMS analysis of granulite facies graphite from Ponmudi, South India. *Earth Planet. Sci. Lett.* **171**, 607-621.
- Ferry J. M. and Baumgartner L. (1987) Thermodynamic models of molecular fluids at the elevated pressures and temperatures of crustal metamorphism. In *Thermodynamic Modeling of Geological Materials: Minerals, Fluids and Melts* (eds. I. S. E.Carmichael and H. P. Eugster). Min. Soc. Am., *Rev. Mineral.* **17**, 323-365.
- Fitton J. G. (1972) The genetic significance of almandine-pyrope phenocrysts in the calc-alkaline Borrowdale Volcanic Group, northern England. *Contrib. Mineral. Petrol.* **36**, 231-248.
- Fortey N. J. (1989) Low grade metamorphism in the Lower Ordovician Skiddaw Group of the Lake District, England. *Proc. Yorks. Geol. Soc.* **47**, 325-337.

- Fortey N. J., Roberts B. and Hirons S. R. (1993) Relationship between metamorphism and structure in the Skiddaw Group, English Lake District. *Geol. Mag.* **130**, 631-638.
- Fortey, N. J., Cooper, A. H., Henney, P. J., Colman, T. and Nancarrow, P. H. A. (1994) Appinitic intrusions in the English Lake District. *Mineral. Petrol.* **51**, 355-375.
- Frost B. R. (1979) Mineral equilibria involving mixed-volatiles in a C-O-H fluid phase: The stabilities of graphite and siderite. *Am. J. Sci.* **279**, 1033-1059.
- Galy V., Beyssac O., France-Lanord C. and Eglinton T. (2008) Selective recycling of graphite during Himalayan erosion: a geological stabilisation of C in the crust. *Science* **322**, 943-945.
- Giammanco, S., Gurrieri, S. and Valenza, M. (1998) Anomalous soil CO₂ degassing in relation to faults and eruptive fissures on Mount Etna (Sicily, Italy). *Bull. Volcanol.* **60**, 252-259.
- Giggenbach W. F. (1996) Chemical composition of volcanic gases. In: Monitoring and mitigation of volcano hazards (eds. R. Scarpa and R.I. Tilling). Springer-Verlag, Berlin. pp. 221-256.
- Giggenbach W. F., Shinohara H., Kusakabe M. and Ohba T. (2003) Formation of acid volcanic brines through interaction of magmatic gases, seawater, and rock within the White Island volcanic-hydrothermal system, New Zealand. In *Volcanic, geothermal, and ore-forming fluids; rulers and witnesses of processes within the Earth* (eds. S. F. Simmons and I. Graham). Special Publication, Society of Economic Geologists **10**, 19-40.
- Graham C.M., Viglino J. A. and Harmon R. S. (1987) Experimental study of hydrogen-isotope exchange between aluminous chlorite and water and of hydrogen diffusion in chlorite. *Am. Mineral.* **72**, 566-579.
- Grew E. S. (1974) Carbonaceous material in some metamorphic rocks of New England and other areas. *J. Geol.* **82**, 5-73.
- Hedenquist J. W. and Lowenstern J. B. (1994) The role of magmas in the formation of hydrothermal ore deposits. *Nature* **370**, 519-527.
- Hedenquist W. and Masahiro A. (1991) Meteoric interaction with magmatic discharges in Japan and the significance for mineralization. *Geology* **19**, 1041-1044.

- Hedenquist, J. W., Matsuhisa Y., Izawa E., White N. C., Giggenbach, W. F. and Aoki, M (1994) Geology, geochemistry, and origin of high sulfidation Cu-Au mineralization in the Nansatsu District, Japan. *Econ. Geol.* **89**, 1-30.
- Henley R. W. and Hedenquist J. W. (1986) Introduction to the geochemistry of active and fossil geothermal system. In *Guide to the active epithermal (geothermal) system and precious metal deposits of New Zealand* (ed. P. J. Roberts). *Monograph Series on Mineral Deposits* **26**, 1-22.
- Huizenga J.M. (2005) COH, an Excel spreadsheet for composition calculations in the C-O-H fluid system. *Comp. Geosc.* **31**, 797-800.
- Jarosewich E., Nelen J. A. and Norberg, J. A. (1980) Reference samples for electron microprobe analysis. *Geostandards Newslett.* **4**, 43-47.
- Judik K., Rantitsch G., Rainer T. M., Árkai P. and Tomljenović B. (2008) Alpine metamorphism of organic matter in metasedimentary rocks from Mt. Medvednica (Croatia). *Swiss J. Geosci.* **101**, 605-616.
- Kribek B., Hrabal J., Landais P. and Hladikova J. (1994) The association of poorly ordered graphite, coke and bitumens in greenschist facies rocks of the Ponikla' group, Lugikum, Czech Republic: the result of graphitization of various types of carbonaceous matter. *J. metamorphic Geol.* **12**, 493-503.
- Lee M. K. (1986) A new gravity survey of the Lake District and three-dimensional model of the granite batholith. *J. Geol. Soc., London* **143**, 425-436.
- Lindgren P. and Parnell J. (2006) Petrographic criteria for fluid mobility of graphitic carbon in terrestrial and extraterrestrial samples. *J. Geochem. Exploration* **91**, 126-129.
- Liou J. G. (1993) Stabilities of natural epidotes. In *Proceedings of the 125 Jahre Kappenwand Symposium* (eds. V. Hock and F. Koller), Vienna. pp. 7-16.
- Lowenstern, J. B. (2001) Carbon dioxide in magmas and implications for hydrothermal systems. *Mineralium Deposita* **36**, 490-502.
- Lowry D., Boyce A. J., Pattick R. A. D., Fallick A. E. and Stanley C. J. (1991) A sulphur isotopic investigation of the potential sulphur sources for Lower Palaeozoic-hosted vein mineralization in the English Lake District. *J. Geol. Soc., London* **148**, 993-1004.
- Luque F. J., Pasteris J. D., Wopenka B., Rodas M. and Barrenechea J. F. (1998) Natural fluid-deposited graphite: mineralogical characteristics and mechanisms of formation. *Am. J. Sci.* **298**, 471-498.

- Luque F. J., Ortega L., Barrenechea, J. F., Millward D., Beyssac O. and Huizenga, J-M. (2009) Deposition of highly crystalline graphite from moderate-temperature fluids. *Geology* **37**, 275-278.
- McConnell B. J., Menuge J. F. and Hertogen J. (2002) Andesite petrogenesis in the Ordovician Borrowdale Volcanic Group of the English Lake District by fractionation, assimilation and mixing. *J. Geol. Soc., London* **159**, 417-424.
- Merriman R. J. (2006) Clay mineral assemblages in British Lower Palaeozoic mudrocks. *Clay Min.* **41**, 473-512.
- Millward, D. (2002). Early Palaeozoic magmatism in the English Lake District. *Proc. Yorks. Geol. Soc.* **54**, 65-93.
- Millward D. (2004) The Caradoc volcanoes of the English Lake District. *Proc. Yorkshire Geol. Soc.* **55**, 73-105.
- Millward D. and Evans J. A. (2003) U-Pb chronology of late Ordovician magmatism in the English Lake District. *J. Geol. Soc., London* **160**, 773-781.
- Mitchell, J. G. and Ineson, P. R. 1975. Potassium-Argon ages from the graphite deposits and related rocks of Seathwaite, Cumbria. *Proc. Yorks. Geol. Soc.* **40**, 413-418.
- Ohmoto H. and Kerrick D. (1977) Devolatilization equilibria in graphitic systems. *Am. J. Sci.* **277**, 1031-1044.
- Okuyama-Kusunose Y. and Itaya T. (1987) Metamorphism of carbonaceous material in the Tono contact aureole, Kitagami Mountains, Japan. *J. metamorphic Geol.* **5**, 121-139.
- Parnell J. (1982) Genesis of the graphite deposit at Seathwaite in Borrowdale, Cumbria. *Geol. Mag.* **119**, 511-512.
- Putnis A., Prieto M. and Fernández-Díaz, L. (1995) Fluid supersaturation and crystallization in porous media. *Geol. Mag.* **132**, 1-13.
- Ramboz C., Pichavant M. and Weisbrod A. (1982) Fluid immiscibility in natural processes. Use and misuse of fluid inclusion data. II. Interpretation of fluid inclusion data in terms of immiscibility. *Chem. Geol.* **37**, 29-48.
- Rantitsch G., Grogger W., Teichert C., Ebner F., Hofer C., Maurer E-M., Schaffer B. and Toth M. (2004) Conversion of carbonaceous material to graphite within the Greywacke Zone of the Eastern Alps. *Internat. J. Earth Sci.* **93**, 959-973.

- Rumble D., Duke E. F. and Hoering T. C. (1986) Hydrothermal graphite in New Hampshire: Evidence of carbon mobility during regional metamorphism. *Geology* **14**, 452-455.
- Santosh M., Wada H., Satish-Kumar M. and Binu-Lal S. S. (2003) Carbon isotope "stratigraphy" in a single graphite crystal; implications for the crystal growth mechanism of fluid-deposited graphite. *Am. Miner.* **88**, 1689-1696.
- Satish-Kumar M. (2005) Graphite-bearing CO₂-fluid inclusions in granulites: Insights on graphite precipitation and carbon isotope evolution. *Geochim. Cosmochim. Acta* **69**, 3841-3856.
- Scheele N. and Hoefs J. (1992) Carbon isotope fractionation between calcite, graphite and CO₂: an experimental study. *Contrib. Mineral. Petrol.* **112**, 35-45.
- Sharp Z. D. (1990) Laser-based microanalytical method for the in situ determination of oxygen isotope ratios of silicates and oxides. *Geochim. Cosmochim. Acta* **54**, 1353-1357.
- Sheppard S. M. F. (1986) Characterization and isotopic variations in natural waters. In *Stable Isotopes in High Temperature Geological Processes* (eds. J. W. Valley, H. P. J. Taylor and J. R. O'Neil). *Rev. Mineral.* **16**, 165-185.
- Soper, N. J. and Woodcock, N. H. (2003) The lost Lower Old Red Sandstone of England and Wales: a record of post-lapetan flexure or Early Devonian transtension? *Geol. Mag.* **140**, 627-647.
- Stone P., Cooper A. H. and Evans J. A. (1999) The Skiddaw Group (English Lake District) reviewed: early Palaeozoic sedimentation and tectonism at the northern margin of Avalonia. In *In Sight of the Suture: the Geology of the Isle of Man in its Iapetus Ocean Context* (eds. N. H. Woodcock, W. R. Fitches, D. G. Quirk and R. P. Barnes). Special Publication 160, Geological Society, London. pp. 325-336.
- Strens R. G. J. (1965) The graphite deposit of Seathwaite in Borrowdale, Cumberland. *Geol. Mag.* **102**, 393-406.
- Valley J. W., Kitchen N., Kohn M. J., Niendorf C. R. and Spicuzza M. J. (1995) UWG-2, a garnet standard for oxygen isotope ratios: Strategies for high precision and accuracy with laser heating. *Geochim. Cosmochim. Acta* **59**, 5223-5231.
- Wada H., Tomita T., Matsuura K., Iuchi K., Ito M. and Morikiyo T. (1994) Graphitization of carbonaceous matter during metamorphism with references

- to carbonate and pelitic rocks of contact and regional metamorphisms, Japan. *Contrib. Mineral. Petrol.* **118**, 217-228.
- Wallace, P. J. (2005) Volatiles in subduction zone magmas: concentrations and fluxes based on melt inclusion and volcanic gas data. *J. Volcanol. Getherm. Res.* **140**, 217-240.
- Ward J. C. (1876) *The geology of the northern part of the English Lake District. Memoir of the Geological Survey of Great Britain.* Quarter Sheet 101SE (England and Wales Sheet 29, Keswick).
- Warr L. N. and Rice H. N. (1994) Interlaboratory standardization and calibration of clay mineral crystallinity and crystallite size data. *J. metamorphic Geol.* **12**, 141-152.
- Weis P. L., Friedman I. and Gleason J. P. (1981) The origin of epigenetic graphite: evidence from isotopes. *Geochim. Cosmochim. Acta* **45**, 2325-2332.

CAPTIONS OF FIGURES

Figure 1. Outline of the geology of the Lake District Lower Palaeozoic Inlier, UK. BCF Burtneess Comb Fault (Millward, 2002).

Figure 2. Orthorectified aerial photograph, geological plan and cross-section of the Borrowdale graphite workings. Aerial photograph © UKP/Getmapping licence No UKP2006/01. The cross-section is a projection of some of the known workings onto a single NW-SE profile and is modified after Ward (1876). The plan shows the extent of some workings on the graphite veins on Gill, Farey's and Gilbert's levels, explored as part of the current study. Level working plans from archives held by the British Geological Survey. Geological information on the plan from the current survey. Fault ticks indicate the downthrow side. The scale of the plan and cross-section is the same as the aerial photograph.

Figure 3. A: Hand specimen of altered diorite containing rounded nodules of graphite. B: Chlorite alteration halo surrounding a graphite nodule within altered diorite. C: Hand specimen showing graphite nodules and one xenolith of Skiddaw Group sandstone. D: Transmitted light photomicrograph of subeuhedral pyrite crystals within altered andesite.

Figure 4. Backscattered image (EPMA) of A) radiating aggregate of epidote crystals

within a graphite nodule, and B: chlorite and graphite from a chlorite-graphite vein. The black material in both images is graphite.

Figure 5. DTA curve of graphite from the Borrowdale deposit, showing the temperature of the exothermic peak due to graphite combustion.

Figure 6. Hand specimen with graphite nodules showing location of the points (white dots) analysed for carbon isotope ratios. The figures in white correspond to the $\delta^{13}\text{C}$ values of each point. Note the homogeneity of the values within a given nodule (except for point G2-07) and the lack of any apparent isotopic zoning.

Figure 7. A: Hand specimen from the mineralized pipes in the Borrowdale deposit. The sample includes graphite (Gph) and an angular quartz fragment (Qtz) within an intensely altered andesite matrix (AA). Small quartz fragments are also embedded within the graphite mass. Photos B to D are transmitted light photomicrographs (B, one polar; C and D, crossed polars). B and C: Polycrystalline internal texture of the quartz fragments, with trails of secondary inclusions within the core (marked by arrows in B). Dark appearance of the grain boundaries is due to the presence of abundant fluid inclusions. Recrystallization of quartz is observed in some boundaries (arrow in C). D: Primary vapour-rich inclusions in bands of recrystallized quartz between quartz grains.

Figure 8. Fluid inclusion types in quartz. V: vapour phase, L: liquid phase, S: solid phase, $\#X\text{CO}_2 = X\text{CO}_2/(X\text{CO}_2 + X\text{CH}_4)$. See text for explanation of fluid inclusion features.

Figure 9. Distribution of fluid inclusions in quartz (transmitted light photomicrographs, one polar). A: Trail of secondary V inclusions, with no visible aqueous phase ($V_v/V_t > 90\%$). B: Type V inclusions with observable aqueous liquid. C: VS inclusions spatially associated with V and L1 inclusions along trails. D: Detail of photo C. The black phase within the inclusion corresponds to highly crystalline graphite. E: L1 and V inclusions occurring in separate but parallel trails. F: Common occurrence of L1 inclusions closely associated with V inclusions. G: Late L2 inclusions trails within the core of the quartz grains. H: L2 inclusions in dark areas of the quartz close to grain boundaries (see Fig. 7B and C).

Figure 10. XH_2O versus $X\text{CO}_2/(X\text{CO}_2 + X\text{CH}_4)$ diagram for bulk compositional data of

V, L1, and L2 inclusions.

Figure 11. Calculated fluid isotope compositions for the Borrowdale graphite deposit in relation to reference waters. The δD_{H_2O} and $\delta^{18}O_{H_2O}$ values calculated from chlorite. The arms of the cross depict the uncertainty of fractionation factors at the estimated temperature (500 °C) and the range of the isotopic values for chlorite (Table 1). Metamorphic water box from Sheppard (1986), magmatic water box from Hedenquist and Lowenstern (1994). The asterisk marks the composition of the reference SMOW water.

Figure 12. A: C-O-H fluid system at 2.5 kbar and 500°C. Open circles indicate fluid fO_2 relative to FMQ. B: Enlargement of the inset in A. Indicated are iso oxygen fugacity lines. The open square relates to carbon supersaturated fluid as a result of hydration reactions. Note that the fluid fO_2 will decrease slightly during water removal. Trajectory 1 corresponds to the precipitation of graphite as result of the reduction of CO_2 at relatively constant fO_2 . During the final stage of graphite precipitation, the dominant graphite precipitation reaction changes and becomes the oxidation of CH_4 (trajectory 2). Shaded areas: compositional fields of the different inclusion types based on $\#CO_2$. The diagram was calculated using an updated version of the Excel spreadsheet COH (Huizenga, 2005).

Figure 13. Carbon stable isotope ratios of graphite from the Borrowdale deposit and of carbonaceous matter from Skiddaw metapelites. The figure outlines the fractionation of the original assimilated carbon as well as the reactions involved through the different stages of graphite deposition. The $\delta^{13}C$ values of individual graphite morphologies are those reported by Barrenechea et al. (2009).

Element	Chlorite 1 (veins) (n=10)	Chlorite 2 (veins) (n=8)	Chlorite (andesite) (n=9)	Element	Epidote (n=12)
SiO ₂	23.86 (0.36)	24.47 (0.27)	27.48 (0.61)	SiO ₂	37.48 (0.46)
Al ₂ O ₃	21.66 (0.38)	21.53 (0.25)	20.57 (0.72)	Al ₂ O ₃	24.02 (0.65)
FeO	32.78 (0.57)	31.24 (0.42)	23.54 (1.31)	Fe ₂ O ₃ *	12.55 (1.10)
MnO	1.90 (0.14)	1.74 (0.08)	0.96 (0.17)	MnO	0.18 (0.08)
MgO	7.28 (0.26)	8.64 (0.43)	13.92 (1.92)	MgO	0.12 (0.07)
CaO	0.03 (0.01)	0.03 (0.01)	0.21 (0.09)	CaO	23.5 (0.84)
Na ₂ O	0.03 (0.02)	0.02 (0.01)	0.03 (0.02)	Na ₂ O	0.01 (0.01)
K ₂ O	0.02 (0.02)	0.01 (0)	0.03 (0.01)	K ₂ O	0.16 (0.09)
TiO ₂	0.036 (0.02)	0.04 (0.01)	0.04 (0.02)	TiO ₂	0.13 (0.06)
NiO	0.02 (0.01)	0.03 (0.02)	0.03 (0.02)	NiO	0.05 (0.03)
Cr ₂ O ₃	0.02 (0.01)	0.02 (0.01)	0.23 (0.14)	Cr ₂ O ₃	0.02 (0.01)
P ₂ O ₅	0.01 (0.01)	0.02 (0.01)	0.12 (0.07)	P ₂ O ₅	0.03 (0.02)
Total	87.63	87.74	87.14	Total	98.2
Si	5.30	5.37	5.79	Si	2.98
Al ^(IV)	2.70	2.63	2.21	Al ^(IV)	0.02
Ti	0.01	0.01	0.01	Ti	0.01
Al ^(VI)	2.97	2.94	2.90	Al ^(VI)	2.25
Fe ²⁺	6.09	5.73	4.15	Fe ³⁺	0.75
Mn	0.36	0.32	0.17	Mn	0.01
Mg	2.41	2.83	4.37	Mg	0.01
Ca	0.01	0.01	0.05	Ca	2.00
Na	0.01	0.01	0.01	Na	0.00
K	0.01	0.00	0.01	K	0.02
				Ps**	25.01

$\delta^{18}\text{O}$ (n=4) = 2.5 (± 0.01) ‰
 δD (n=11) = -63.4 (± 0.4) ‰

* Total Fe as Fe₂O₃

** Ps=100(Fe³⁺/Fe³⁺+Al^(VI))

n = number of analyses

Sample	$\delta^{13}\text{C}$ (‰)
PO-05	-26.9
PO-06	-25.8
G2-01	-25.0
G2-02	-26.2
G2-03	-26.2
G2-04	-26.1
G2-05	-26.4
G2-06	-26.5
G2-07	-23.4
G2-08	-27.4
G2-09	-27.4
G2-10	-26.5
G2-11	-27.1
G2-12	-26.6
G2-13	-26.6
G4	-27.1
G6	-26.3
GB3	-28.3
GB9	-28.3
P2-1	-26.3
F1-1	-26.4
F1-2	-26.3

Sample	Elemental Carbon (%)	$\delta^{13}\text{C}_{\text{V-PDB}}$ (‰)	
SK-1-1 (<53 μm)	0.21	-28.41	-28.34
SK-1-2 (<53 μm)	0.28	-27.78	-27.85
SK-1-3 (<25 μm)	0.86	-24.35	-24.38
SK-2-1 (<53 μm)	0.36	-29.86	-30.07
SK-2-2 (<53 μm)	0.36	-30.12	-30.09
SK-2-3 (<25 μm)	0.73	-28.14	-28.05
SK-3-1 (<53 μm)	0.18	-27.27	-27.38
SK-3-2 (<53 μm)	0.19	-27.41	-27.35
SK-3-3 (<25 μm)	0.31	-23.57	-23.41

		Raman data		Microthermometric data				Bulk compositional data					
	Vv/Vt	XCO ₂	XCH ₄	ThCO ₂	Tm ice	TmCl	TH	XH ₂ O	XCO ₂	XCH ₄	Salinity	Molar Vol	Density
Type V													
	0.7	0.67	0.33	-1.9 L	-	+14.4	293 *	0.64	0.24	0.12	1.4	40.15	0.60
	0.8	0.64	0.36	+0.5 L	-	-	332 V	0.53	0.30	0.17	-	49.37	0.52
	0.5	0.75	0.25	+7.9 L	-	-	340 C	0.79	0.16	0.05	-	29.84	0.74
	0.7	0.75	0.25	+3.8 L	-	+14.2	300 *	0.63	0.28	0.09	0.3	39.43	0.64
	0.7	0.60	0.30	-8.1 L	-	+14.2	349 C	0.66	0.21	0.13	2.9	40.88	0.57
	0.6	0.77	0.23	+2.7 L	-	-	275 *	0.72	0.22	0.06	-	33.68	0.70
	0.7	0.75	0.25	+3.3 L	-	+14.2	321 V	0.63	0.28	0.09	0.4	39.39	0.64
	0.6	0.81	0.19	+3.1 L	-	-	273 *	0.71	0.24	0.05	-	33.32	0.73
	0.6	0.69	0.31	+4.1 L	-	-	338 V	0.73	0.19	0.08	-	34.40	0.66
	0.9	0.77	0.23	+3.1 L	-	-	270 *	0.31	0.54	0.16	-	57.62	0.55
	0.7	0.62	0.38	-9.9 L	-	-	267 *	0.65	0.22	0.13	-	40.46	0.58
	0.95	0.68	0.32	-23.6 L	-	-	-	0.18	0.56	0.26	-	66.35	0.48
	0.95	0.74	0.26	-13.6 L	-	-	-	0.17	0.61	0.22	-	64.20	0.52
	0.95	0.72	0.28	-8.0 L	-	-	-	0.18	0.59	0.23	-	65.95	0.50
Type L1													
	0.2	0.14	0.86	-	-7.0	10.5	276 L	0.967	0.009	0.024	8.1	21.92	0.86
	0.15	0.21	0.79	-	-6.1	10.5	-	0.973	0.012	0.015	7.3	20.53	0.89
	0.30	0.28	0.72	-	-6.7	9.0	321 L	0.958	0.019	0.023	7.2	20.90	0.75
	0.4	0.50	0.50	-	-7.2	10.5	372 L	0.930	0.043	0.027	5.7	29.01	0.67
	0.25	0.60	0.40	-	-5.5	11.1	220*	0.949	0.038	0.013	5.0	23.84	0.81
	0.25	0.62	0.38	-	-6.0	10.5	283 *	0.950	0.039	0.011	5.6	23.91	0.81
	0.2	0.03	0.97	-	-4.2	16.0	342 L	0.953	0.003	0.044	4.4	21.39	0.85
	0.6	0.20	0.80	-	-7.1	9.5	348 L	0.902	0.025	0.073	4.0	41.21	0.46
	0.3	0.14	0.86	-	-5.9	10.5	290 L	0.955	0.011	0.034	6.3	24.77	0.75
Type L2													
	0.1	-	1	-	-5.1	-	195	0.98	-	0.02	8.0	19.07	0.97
	0.1	-	1	-	-4.3	-	179	0.98	-	0.02	6.9	19.13	0.96
	0.1	-	1	-	-3.7	-	183	0.98	-	0.02	6.0	19.18	0.96
	0.1	-	1	-	-4.1	-	188	0.98	-	0.02	6.6	19.15	0.96

Raman, microthermometric and calculated compositional data of selected fluid inclusions from Borrowdale.

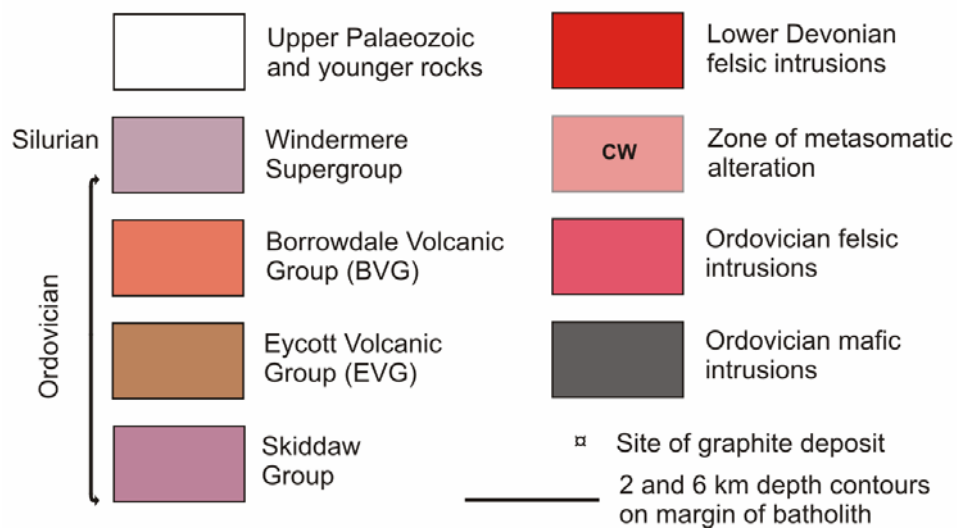
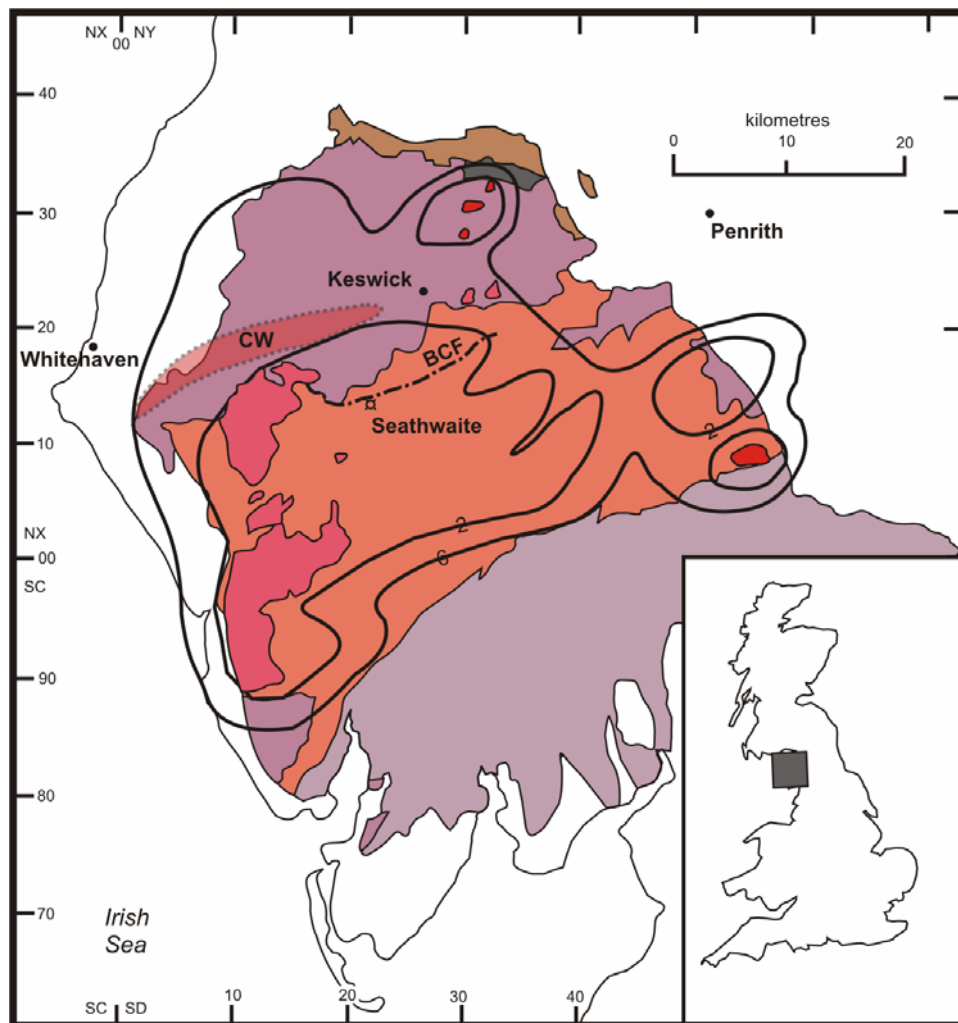


Figure 1

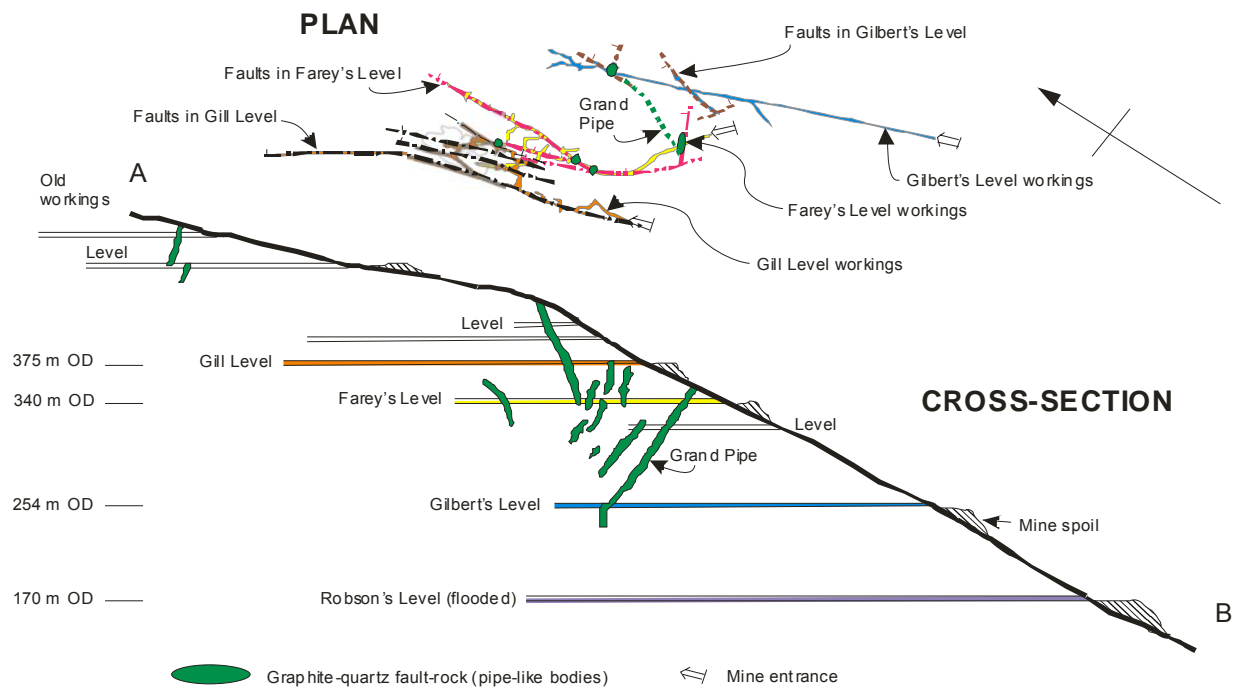
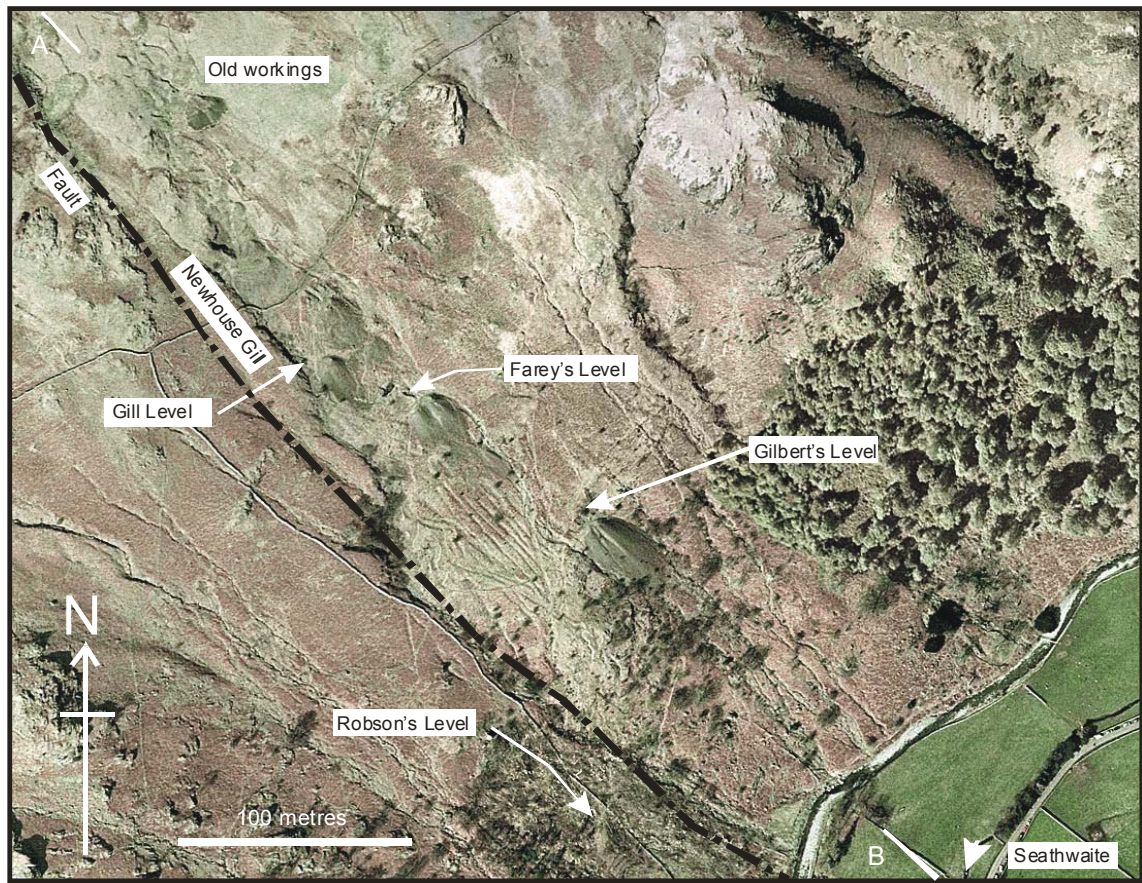


Figure 2

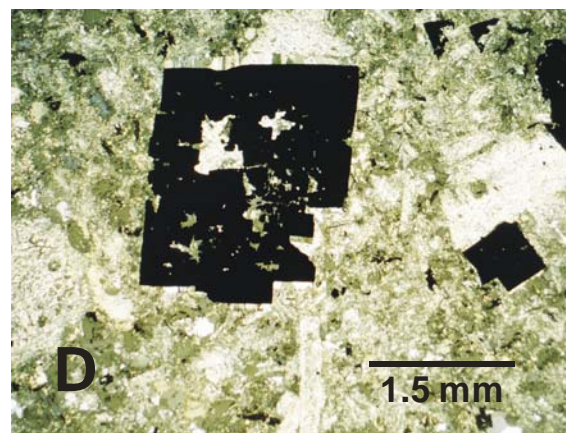
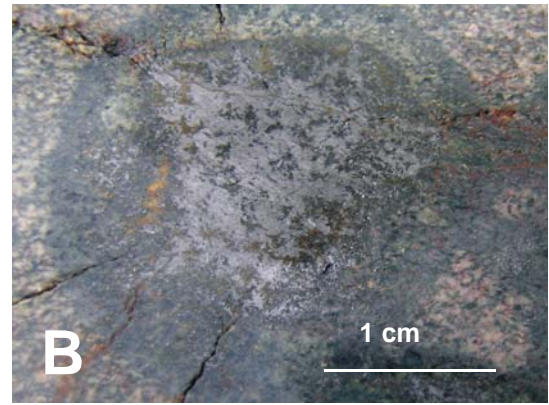


Figure 3

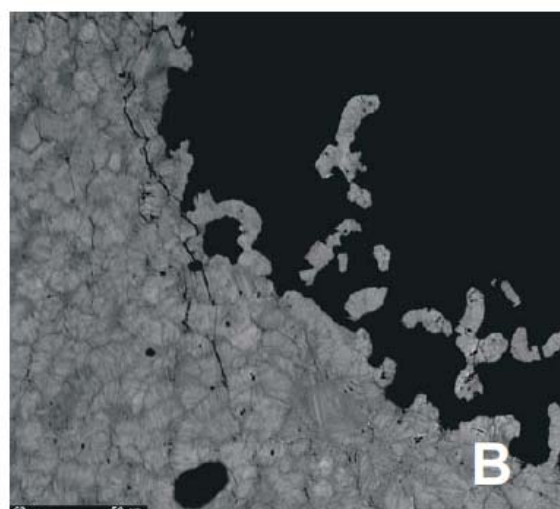
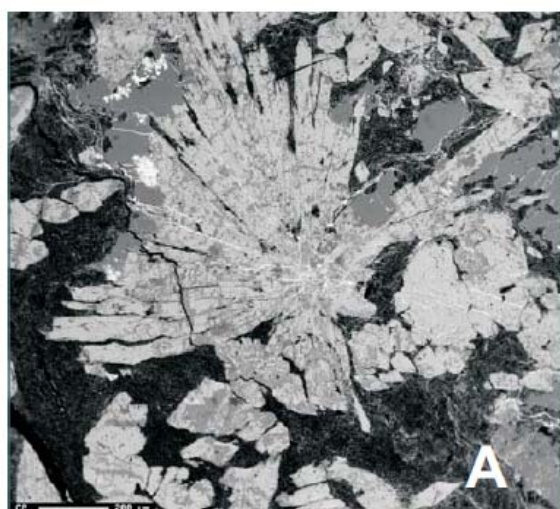


Figure 4

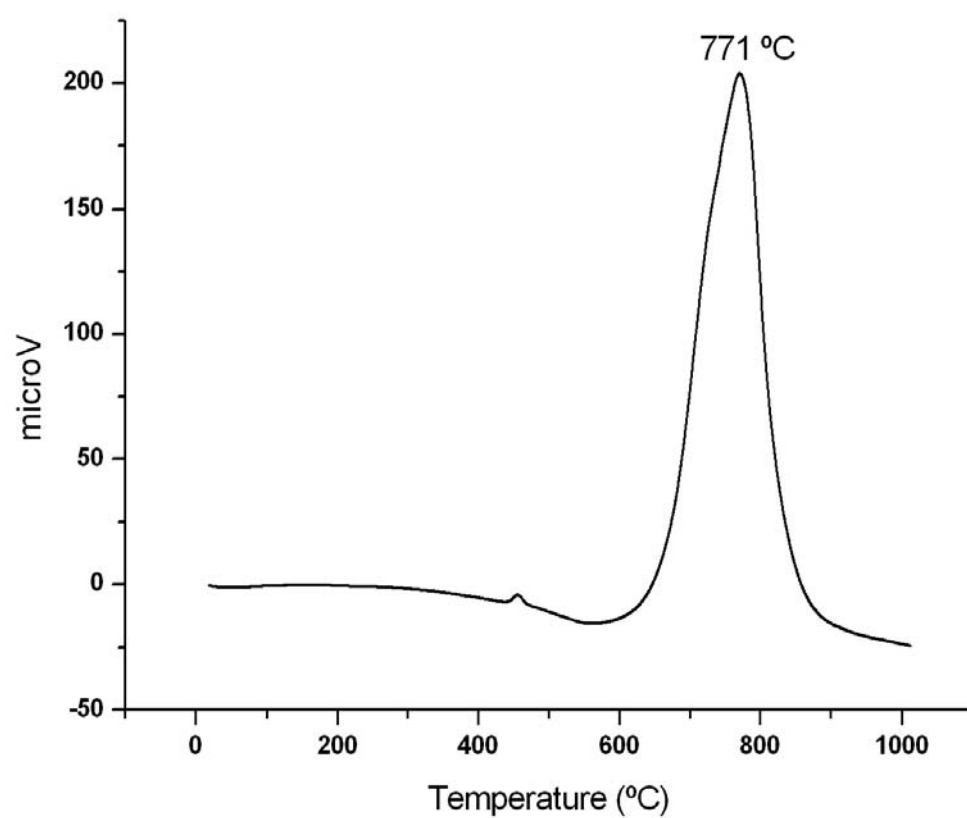


Figure 5

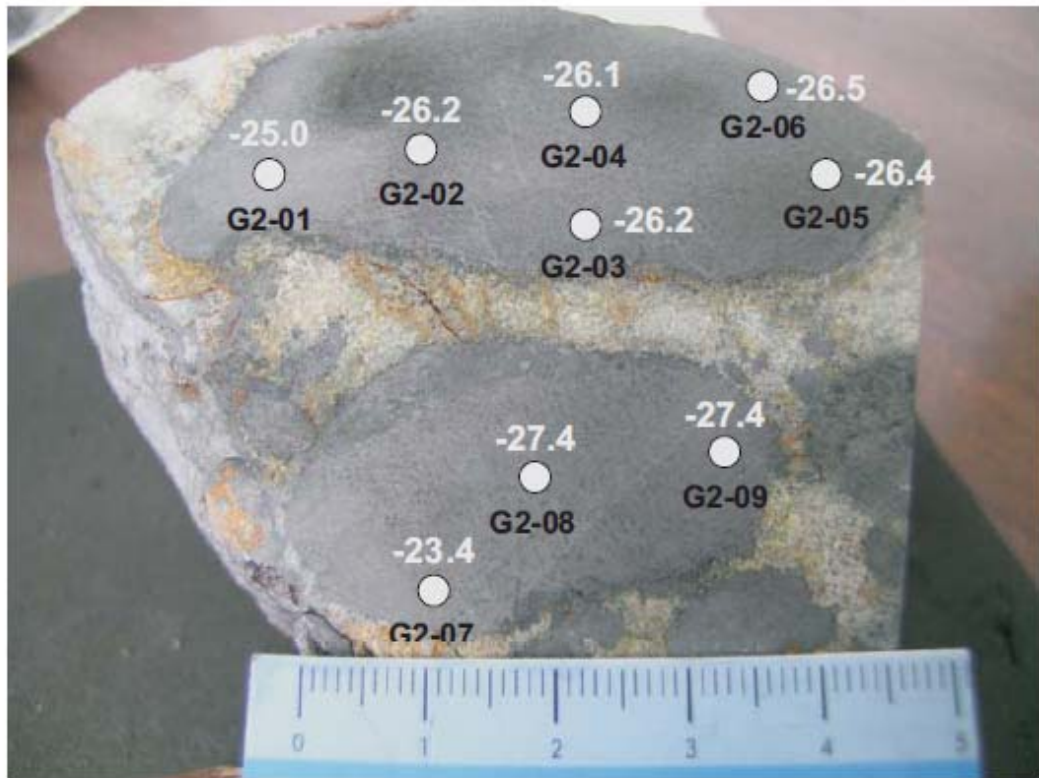


Figure 6

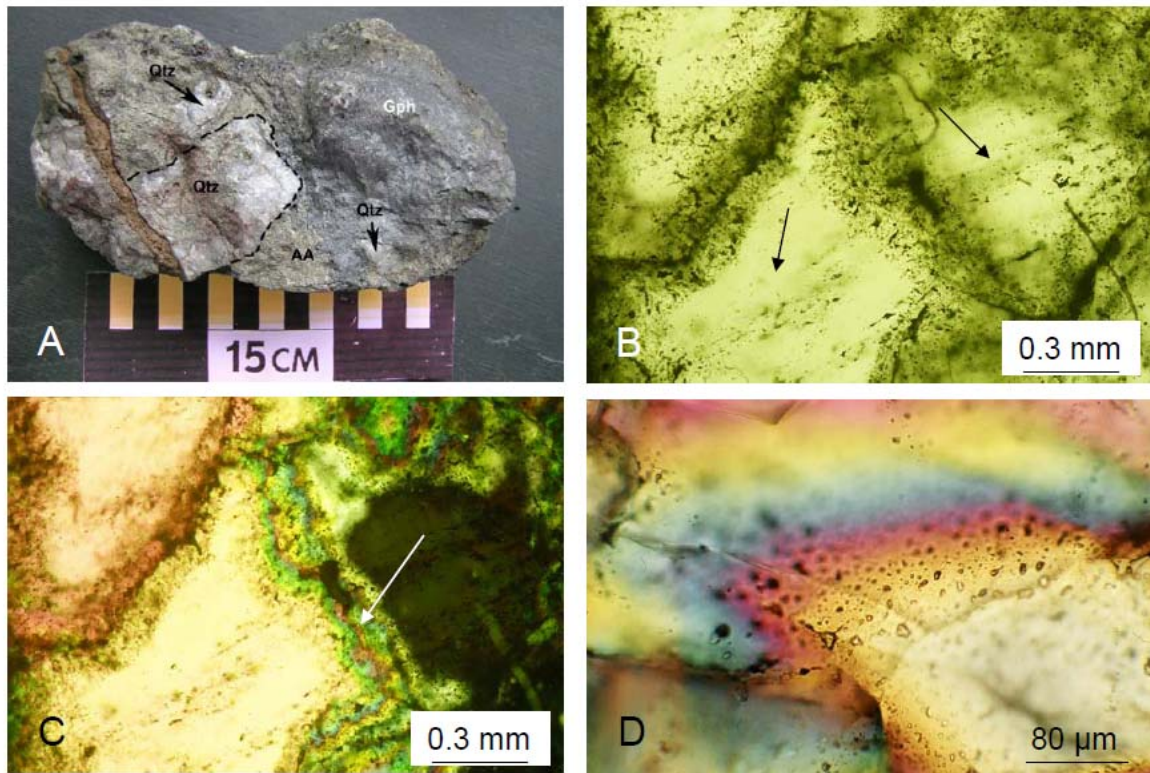


Figure 7

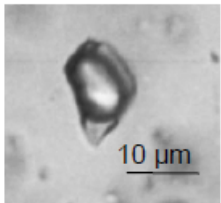
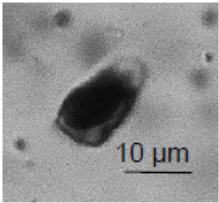
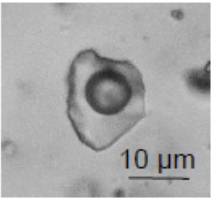
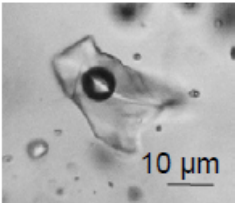
V	VS	L1	L2
 <p> $V_{\text{CO}_2\text{-CH}_4} + L_{\text{H}_2\text{O}}$ $\#X_{\text{CO}_2} = 0.6 - 0.8$ </p>	 <p> $V_{\text{CH}_4} + L_{\text{H}_2\text{O}} + S_{\text{C}}$ $\#X_{\text{CO}_2} = 0$ </p>	 <p> $L_{\text{H}_2\text{O}} + V_{\text{CO}_2\text{-CH}_4}$ $\#X_{\text{CO}_2} = 0.03 - 0.6$ </p>	 <p> $L_{\text{H}_2\text{O}} + V_{\text{CH}_4}$ $\#X_{\text{CO}_2} = 0$ </p>

Figure 8

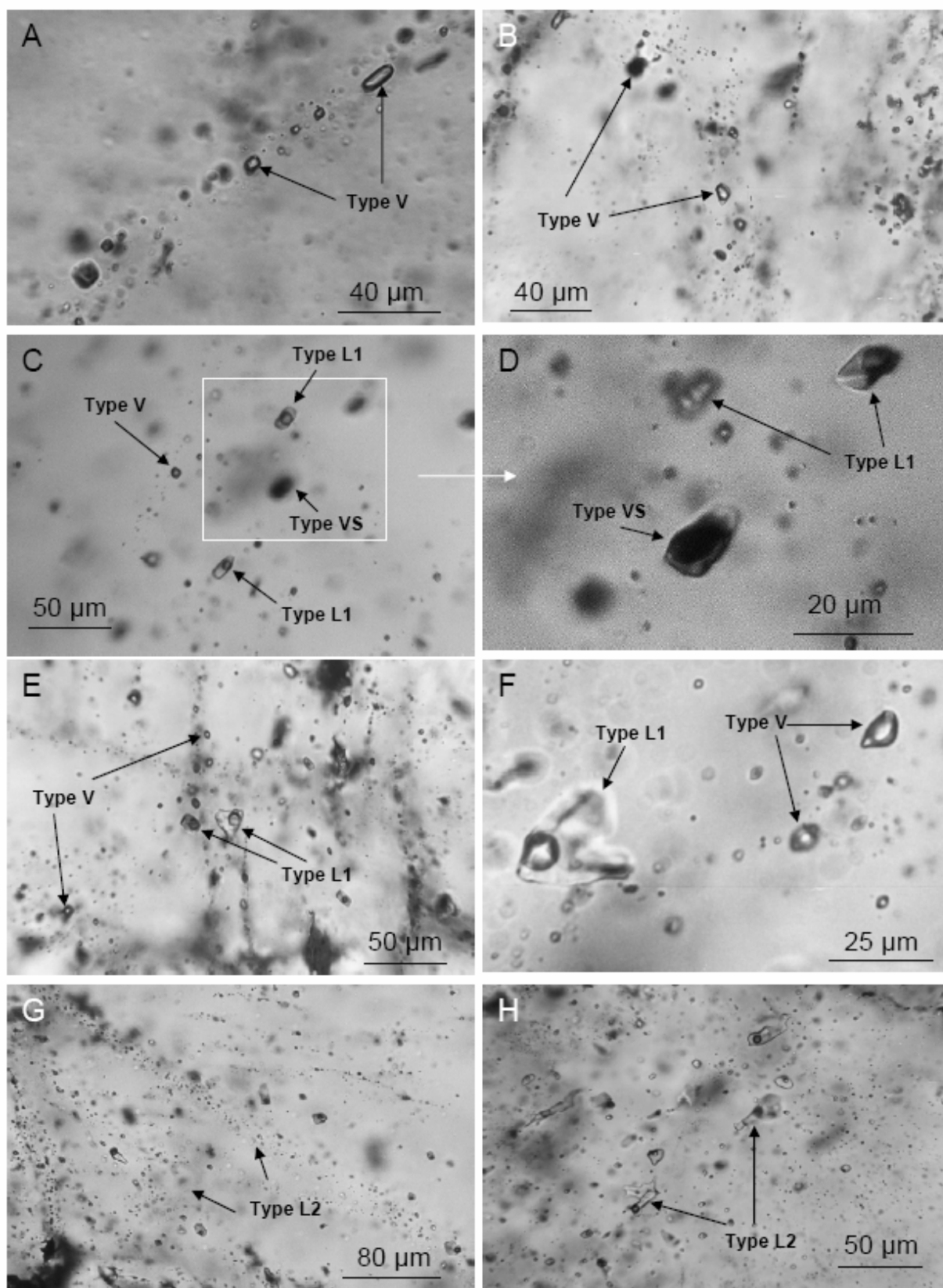


Figure 9

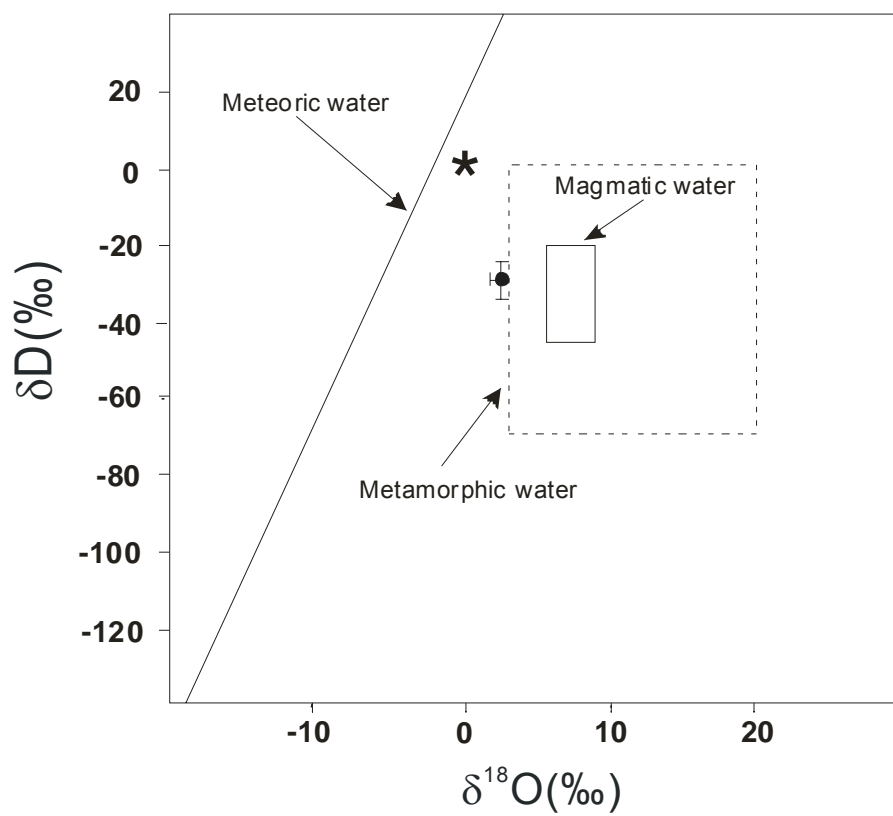


Figure 10

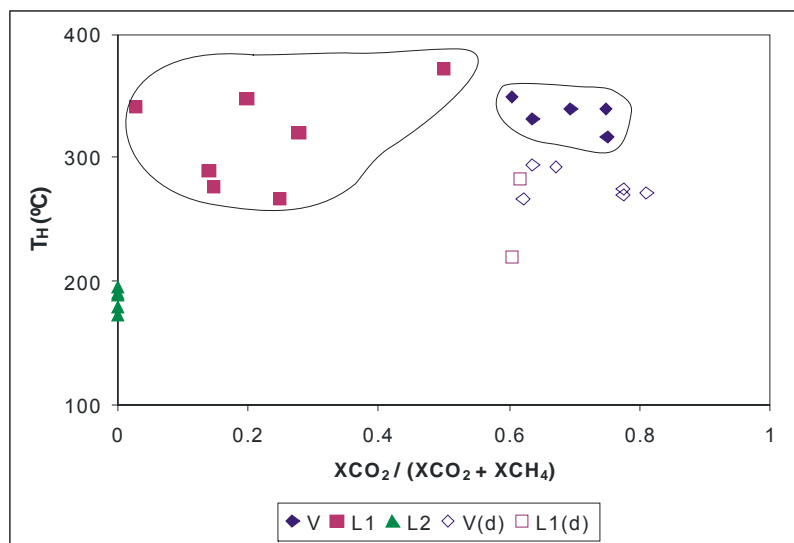


Figure 11

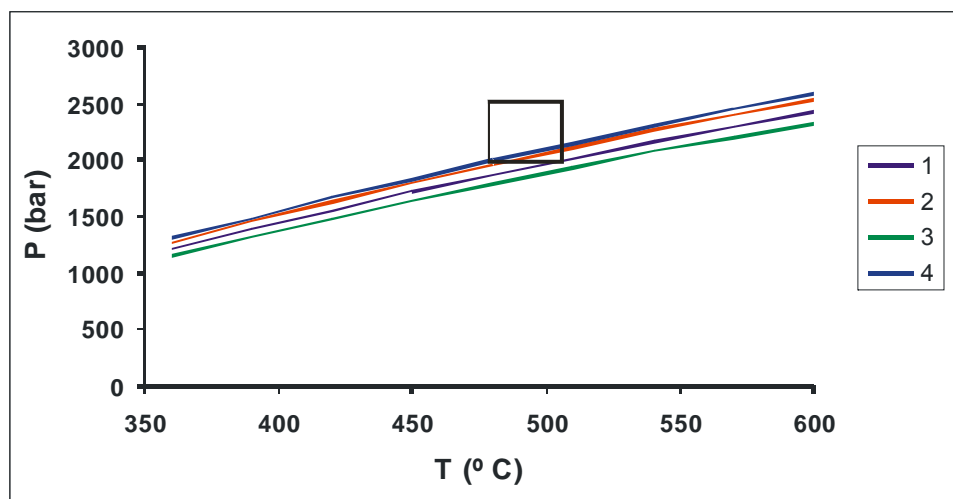


Figure 12

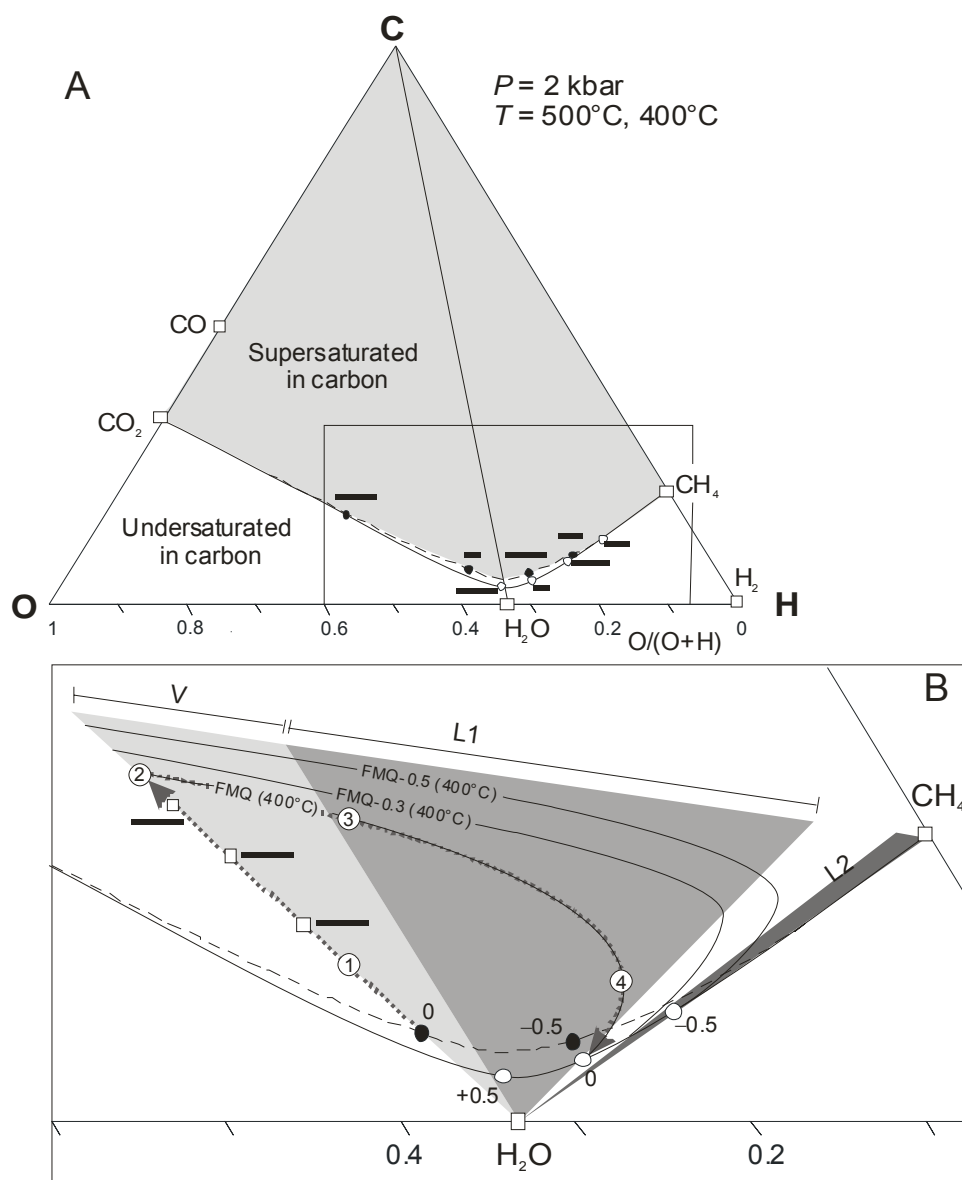


Figure 13

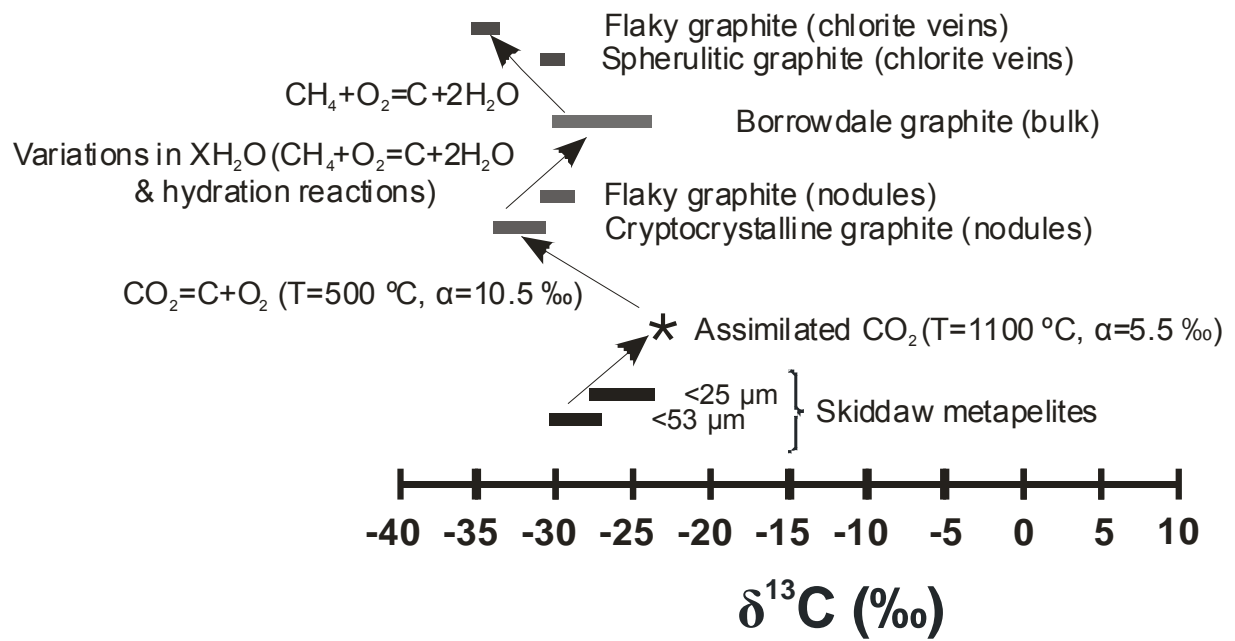


Figure 14

Table 1. Chemical and stable isotope composition of minerals from the Borrowdale deposit

Element	Chlorite 1 (veins) (n=10)	Chlorite 2 (veins) (n=8)	Chlorite (andesite) (n=9)	Element	Epidote (n=12)
SiO ₂	23.86 (0.36)	24.47 (0.27)	27.48 (0.61)	SiO ₂	37.48 (0.46)
Al ₂ O ₃	21.66 (0.38)	21.53 (0.25)	20.57 (0.72)	Al ₂ O ₃	24.02 (0.65)
FeO	32.78 (0.57)	31.24 (0.42)	23.54 (1.31)	Fe ₂ O ₃ ^a	12.55 (1.10)
MnO	1.90 (0.14)	1.74 (0.08)	0.96 (0.17)	MnO	0.18 (0.08)
MgO	7.28 (0.26)	8.64 (0.43)	13.92 (1.92)	MgO	0.12 (0.07)
CaO	0.03 (0.01)	0.03 (0.01)	0.21 (0.09)	CaO	23.5 (0.84)
Na ₂ O	0.03 (0.02)	0.02 (0.01)	0.03 (0.02)	Na ₂ O	0.01 (0.01)
K ₂ O	0.02 (0.02)	0.01 (0)	0.03 (0.01)	K ₂ O	0.16 (0.09)
TiO ₂	0.036 (0.02)	0.04 (0.01)	0.04 (0.02)	TiO ₂	0.13 (0.06)
NiO	0.02 (0.01)	0.03 (0.02)	0.03 (0.02)	NiO	0.05 (0.03)
Cr ₂ O ₃	0.02 (0.01)	0.02 (0.01)	0.23 (0.14)	Cr ₂ O ₃	0.02 (0.01)
P ₂ O ₅	0.01 (0.01)	0.02 (0.01)	0.12 (0.07)	P ₂ O ₅	0.03 (0.02)
Total	87.63	87.74	87.14	Total	98.2
Si	5.30	5.37	5.79	Si	2.98
Al ^(IV)	2.70	2.63	2.21	Al ^(IV)	0.02
Ti	0.01	0.01	0.01	Ti	0.01
Al ^(VI)	2.97	2.94	2.90	Al ^(VI)	2.25
Fe ²⁺	6.09	5.73	4.15	Fe ³⁺	0.75
Mn	0.36	0.32	0.17	Mn	0.01
Mg	2.41	2.83	4.37	Mg	0.01
Ca	0.01	0.01	0.05	Ca	2.00
Na	0.01	0.01	0.01	Na	0.00
K	0.01	0.00	0.01	K	0.02
				Ps^b	25.01
	$\delta^{18}\text{O}$ (n=4) = 2.5 (± 0.01) ‰				
	δD (n=11) = - 63.4 (± 0.4) ‰				

(a) Total Fe as Fe₂O₃

(b) Ps=100(Fe³⁺/Fe³⁺+Al^{VI})

n = number of analyses; standard deviation is given in brackets

Table 2. Bulk stable carbon isotope ratios of selected graphite samples. P: Samples from the Grand Pipe, G: Samples from Gill's level, GB: Samples from Gilbert's level, F: Samples from Farey's level (chlorite-graphite veins)

Sample	$\delta^{13}\text{C}$ (‰)
P0-05	-26.9
P0-06	-25.8
G2-01	-25.0
G2-02	-26.2
G2-03	-26.2
G2-04	-26.1
G2-05	-26.4
G2-06	-26.5
G2-07	-23.4
G2-08	-27.4
G2-09	-27.4
G2-10	-26.5
G2-11	-27.1
G2-12	-26.6
G2-13	-26.6
G4	-27.1
G6	-26.3
GB3	-28.3
GB9	-28.3
P2-1	-26.3
F1-1	-26.4
F1-2	-26.3

Table 4. Replicate stable carbon isotope analyses of Skiddaw metapelites

Sample	$\delta^{13}\text{C}_{\text{V-PDB}}$ (‰)	
SK-1-1 (<53 μm)	-28.41	-28.34
SK-1-2 (<53 μm)	-27.78	-27.85
SK-1-3 (<25 μm)	-24.35	-24.38
SK-2-1 (<53 μm)	-29.86	-30.07
SK-2-2 (<53 μm)	-30.12	-30.09
SK-2-3 (<25 μm)	-28.14	-28.05
SK-3-1 (<53 μm)	-27.27	-27.38
SK-3-2 (<53 μm)	-27.41	-27.35
SK-3-3 (<25 μm)	-23.57	-23.41

Table 3. Raman, microthermometric and calculated compositional data of selected fluid inclusions from Borrowdale (for abbreviations, see text)

	Raman data		Microthermometric data				Bulk compositional data					
Vv/Vt	XCO ₂	XCH ₄	Th _{CAR}	Tm _{ICE}	Tm _{CL}	Th _{TOT}	XH ₂ O	XCO ₂	XCH ₄	Salinity	Molar Vol	Density
Type V												
0.7	0.67	0.33	-1.9 L	-	+14.4	293 *	0.64	0.24	0.12	1.4	40.15	0.60
0.8	0.64	0.36	+0.5 L	-	-	332 V	0.53	0.30	0.17	-	49.37	0.52
0.5	0.75	0.25	+7.9 L	-	-	340 C	0.79	0.16	0.05	-	29.84	0.74
0.7	0.75	0.25	+3.8 L	-	+14.2	300 *	0.63	0.28	0.09	0.3	39.43	0.64
0.7	0.60	0.30	-8.1 L	-	+14.2	349 C	0.66	0.21	0.13	2.9	40.88	0.57
0.6	0.77	0.23	+2.7 L	-	-	275 *	0.72	0.22	0.06	-	33.68	0.70
0.7	0.75	0.25	+3.3 L	-	+14.2	321 V	0.63	0.28	0.09	0.4	39.39	0.64
0.6	0.81	0.19	+3.1 L	-	-	273 *	0.71	0.24	0.05	-	33.32	0.73
0.6	0.69	0.31	+4.1 L	-	-	338 V	0.73	0.19	0.08	-	34.40	0.66
0.9	0.77	0.23	+3.1 L	-	-	270 *	0.31	0.54	0.16	-	57.62	0.55
0.7	0.62	0.38	-9.9 L	-	-	267 *	0.65	0.22	0.13	-	40.46	0.58
0.95	0.68	0.32	-23.6 L	-	-	-	0.18	0.56	0.26	-	66.35	0.48
0.95	0.74	0.26	-13.6 L	-	-	-	0.17	0.61	0.22	-	64.20	0.52
0.95	0.72	0.28	-8.0 L	-	-	-	0.18	0.59	0.23	-	65.95	0.50
Type L1												
0.2	0.14	0.86	-	-7.0	10.5	276 L	-	-	-	8.1	-	-
0.15	0.21	0.79	-	-6.1	10.5	-	-	-	-	7.3	-	-
0.30	0.28	0.72	-	-6.7	9.0	321 L	-	-	-	7.2	-	-
0.4	0.50	0.50	-	-7.2	10.5	372 L	-	-	-	5.7	-	-
0.25	0.60	0.40	-	-5.5	11.1	220*	-	-	-	5.0	-	-
0.25	0.62	0.38	-	-6.0	10.5	283 *	-	-	-	5.6	-	-
0.2	0.03	0.97	-	-4.2	16.0	342 L	-	-	-	4.4	-	-
0.6	0.20	0.80	-	-7.1	9.5	348 L	-	-	-	4.0	-	-
0.3	0.14	0.86	-	-5.9	10.5	290 L	-	-	-	6.3	-	-
Type L2												
0.1	-	1	-	-5.1	-	195	0.98	-	0.02	8.0	19.07	0.97
0.1	-	1	-	-4.3	-	179	0.98	-	0.02	6.9	19.13	0.96
0.1	-	1	-	-3.7	-	183	0.98	-	0.02	6.0	19.18	0.96
0.1	-	1	-	-4.1	-	188	0.98	-	0.02	6.6	19.15	0.96